Regionalized protein localization domains in the zebrafish hair cell kinocilium.

Timothy Erickson [1, *], William Paul Biggers III [2], Kevin Williams [2], Shyanne E. Butland [1], and Alexandra Venuto [2]

[1] Department of Biology, University of New Brunswick, Fredericton, NB E3B 5A3, Canada

[2] Department of Biology, East Carolina University, Greenville, NC 27858, USA

*Correspondence: timothy.erickson@unb.ca

Abstract:

Sensory hair cells are the receptors for auditory, vestibular, and lateral line sensory organs in vertebrates. These cells are distinguished by "hair"-like projections from their apical surface collectively known as the hair bundle. Along with the staircase arrangement of actin-filled stereocilia, the hair bundle features a single, non-motile, true cilium called the kinocilium. The kinocilium plays important roles in bundle development and the mechanics of sensory detection. To understand more about kinocilial development and structure, we performed a transcriptomic analysis of zebrafish hair cells looking for cilia-associated genes that have yet to be characterized in hair cells. Here, we focus on three such genes - *ankef1a*, *odf3l2a*, and *saxo2* - because the human or mouse orthologs are either associated with sensorineural hearing loss or are located near uncharacterized deafness loci. We made transgenic fish that express fluorescently tagged versions of their proteins, demonstrating their localization to the kinocilia of zebrafish hair cells. Furthermore, we find that Ankef1a, Odf3l2a, and Saxo2 exhibit distinct localization patterns along the length of the kinocilium and within the cell body. Lastly, we report a novel overexpression phenotype for Saxo2. Overall, these results suggest that the hair cell kinocilium is regionalized along its proximal-distal axis and set the groundwork to understand more about the roles of these kinocilial proteins in hair cells.

Keywords:

hair cells; kinocilium; cilia; deafness; hearing loss; lateral line; transcriptomics; TU-tagging; zebrafish; ANKEF1; ODF3L2; SAXO2

1. Introduction

Our senses of hearing and balance rely on the function of sensory receptors in our ears called hair cells. Sensory hair cells are distinguished by hair-like projections from their apical surface that detect and transduce physical stimuli such as sound waves or head movements. Most of these projections are actin-filled microvilli (called stereocilia) that form the characteristic stair-cased hair bundle. However, at some point in their development, all vertebrate hair cells also feature a single microtubule-based projection called the kinocilium.

Cilia play prominent roles in sensory cell development and function from an evolutionarily diverse set of organisms [1,2]. In mechanosensory hair cells, the kinocilium can fulfil both sensory and structural roles, depending on the type of hair cell. Although kinocilia degenerate around the onset of hearing in mammalian cochlear hair cells, they nonetheless play a developmental role in establishing hair bundle polarity in the auditory system [3] and mediating Sonic Hedgehog signaling to instruct cochlear development [4,5]. In contrast to the transient kinocilia of cochlear hair cells, the kinocilium is a permanent and prominent feature of most other vertebrate hair cells in the auditory, vestibular, and lateral line organs, including vestibular hair cells of mammals. In non-cochlear cells, it appears that kinocilia play a less pronounced role in establishing bundle polarity. However, they contribute to the structure and functional mechanics of the sensory hair bundle [6–8], as well as act as attachment points for inert masses such as otoliths and otoconia [9]. Kinocilial dynamics may also be involved in the repair and regeneration of cochlear hair cells [10]. As such, characterizing functional components of the kinocilium is fundamental to our understanding of sensory hair cells.

Hair cell kinocilia possess several features that distinguish them from both non-motile, primary cilia and from motile cilia and flagella. Although "kino-" means "motion" and kinocilia usually possess the "9+2" arrangement of axonemal microtubules typically found in motile cilia [11], the hair cell cilium is non-motile, lacking the inner dynein arms and nexin links found in motile cilia [12]. In this respect, kinocilia are similar to some mammalian olfactory cilia, which also have a 9+2 axoneme but lack the dynein machinery to generate motion [13]. However, given the impressive diversity of vertebrate hair cells, it is possible that active movement is a feature of some kinocilia [14,15]. In some contexts, non-"9+2" arrangements of microtubules have also been reported [10,12]. Like hair cells themselves, there is great diversity in kinocilial morphology - from the transient kinocilia of cochlear hair cells, to the bulbed kinocilia of amphibian hair cells, to the towering kinocilia of superficial lateral line neuromasts (and everything in between). However, little is known about the molecular bases for this diversity.

Sensorineural hearing loss can result from mutations in cilia-associated genes as part of a syndromic ciliopathy, such as reported for Alström, Bardet-Biedl, and Usher syndromes [16–18]. Cilia- and microtubule associated genes are also implicated in nonsyndromic hearing loss, examples being *CCDC50* [19], *MAP1B* [20], and *DCDC2* [21]. *PCDH15* and *CDH23* are also examples of cilia-associated Usher proteins where certain alleles result in nonsyndromic hearing loss [22–24]. There may be other cilia-associated genes waiting to be identified that contribute to auditory and / or vestibular function.

To characterize putative kinocilial genes, we have turned to the zebrafish model system. Zebrafish hair cells are genetically and molecularly related to mammalian hair cells [25]. This allows us to utilize the genetic tractability of zebrafish to characterize protein

localization and function for putative human deafness genes. Here, we identify hair cell-enriched transcripts by TU-tagging and focus on three putative kinocilial genes within the dataset - *ankef1a*, *odf3l2a*, and *saxo2* - because of their potential involvement in hearing loss. Mouse *Ankef1* lies within the coloboma (*Cm*) deletion locus whose phenotypes include auditory and vestibular deficits [26,27]. The Shared Harvard Inner Ear Database (SHIELD) reports that human *ODF3L2* and *SAXO2* lie within deafness loci DFNB72 and DFNA30, respectively [28]. We have made transgenic fish that express tagged Ankef1a, Odf3l2a, and Saxo2 proteins and demonstrate their distinct localization patterns within the kinocilium of zebrafish hair cells. Our results set the groundwork for future studies to understand the role of these kinocilial proteins in hair cell structure and function.

2. Methods

2.1. Animal husbandry

Adult zebrafish were maintained and bred using standard procedures [29]. Larval fish were grown at 28.5ºC on a 14:10 hour light cycle in 100 mm Petri dishes containing E3 media (5 mM NaCl, 0.17 mM KCl, 0.33 mM CaCl2 and 0.33 mM MgSO4 buffered with NaHCO3).

2.2. Transgenic fish lines

The *Tg(myo6b:EGFP)vo68*, *Tg(myo6b:actb1-EGFP)vo8* and *Tg(myo6b:yfp-Hsa.TUBA)idc16* transgenic lines have been previously described [8,30,31] and were gifts from the lab of Teresa Nicolson. For the TU-tagging experiments, we used a *Tg(myo6b:HA-UPRT-P2A-NLS-mCherry)* line that was similar to, but distinct from, the *Tg(myo6b:HA-UPRT-P2A-mCherry)* line used previously [32]. The *Tg(myo6b:ankef1a-emGFP)unb4*, *Tg(myo6b:odf3l2a-emGFP)unb5*, *Tg(myo6b:saxo2-emGFP)unb6*, and *Tg(myo6b:saxo2-mKate2)unb7* lines were generated for this study. For the sake of simplicity, we refer to these lines as Ankef1a-GFP, Odf3l2a-GFP, Saxo2-GFP, and Saxo2-mKate2 throughout the manuscript. Coding sequences were amplified using total RNA from 7 days post-fertilization (dpf) zebrafish using the SuperScript IV One-step RT-PCR kit (ThermoFisher) using the primers listed in Table S1. Entry and Destination constructs were made using standard Tol2 Gateway cloning protocols [33].

2.3. Thiouracil (TU)-tagging and bioinformatics

TU-tagging experiments were performed essentially as previously described [32] with the following modifications. Transgenic and wild type sibling larvae from outcrosses of a *Tg(myo6b:HA-UPRT-P2A-NLS-mCherry)* (abbreviated *Tg(UPRT)*) line were used. Stock solutions of 4-thiouracil (4TU; Sigma-Aldrich 440736) and 4-thiouridine (4sU; Sigma-Aldrich T4509) were prepared at 0.5 M and 0.25 M, respectively in DMSO (Sigma-Aldrich D8418). Working solutions were diluted in E3 media with a final DMSO concentration of 0.5%. At 4 dpf, *Tg(UPRT)* larvae were treated with 2 mM 4TU while non-transgenic siblings were treated with 1 mM 4sU. Both groups were bathed in their respective compounds for 3.5 hours at 29ºC. Conversion of 4TU to 4-thiouridine monophosphate is enhanced in the presence of the *Toxoplasma gondii* UPRT enzyme while endogenous biosynthetic pathways can make 4-thiouridine monophosphate directly from 4sU. With this strategy, TU-tagged RNA is preferentially synthesized in the hair cells of *Tg(UPRT)* larvae treated with 4TU while RNA is tagged without bias for cell type in 4sU-treated, non-

transgenic controls. The experiment was performed in biological replicate where a biological sample is defined as 100 larvae per treatment group produced by a single breeding event.

Samples were processed in TRIzol reagent (Ambion 15596026) according to the manufacturer's protocol and enriched for polyadenylated mRNA using the Dynabeads Oligo(dT)25 kit (Ambion 61005). Biotinylation of the mRNA was done using the MTSEA-biotin-XX reagent (Biotium 90066). A 5 mg/ml solution was prepared in *N,N*-Dimethylformamide (DMF; Sigma-Aldrich 227056). A 10X biotinylation buffer was prepared by diluting 1 M Tris-HCl pH 7.5 (ThermoFisher 15567027) to 100 mM and 0.5 M EDTA pH 8 (ThermoFisher AM9261) to 10 mM in nuclease-free water (ThermoFisher AM9930). The biotinylation reaction was performed by heating the mRNA in a 1X biotinylation buffer solution at 65ºC for 2 minutes before adding 10 µg of MTSEA-biotin-XX solution with a final DMF concentration of 25%. Samples were incubated in the dark at room temperature for 30 minutes on a rotating rack. mRNA was recovered by adding an equal volume of chloroform:isoamyl alcohol 24:1 (Sigma-Aldrich C0549), vortexing, retrieving the aqueous phase with 5Prime Phase Lock Gel (Heavy) microfuge tubes, and performing a NaCl-isopropanol precipitation with glycogen (ThermoFisher R0551) acting as an inert carrier. Biotinylated RNA was fragmented to approximately 200 – 500 bases with the NEBNext Magnesium RNA Fragmentation Module (New England Biolabs E6150S) and precipitated by adding 1/10 volume of 3M sodium acetate pH 5.5 (ThermoFisher AM9740) plus 3 volumes of 100% ethanol, again with glycogen as an inert carrier. Finally, biotinylated TU-tagged RNA was separated from untagged RNA using the µMacs Streptavidin kit (Miltenyi Biotec 130-074-101). High salt MPG buffer (100 mM Tris, 10 mM EDTA, 1 M NaCl, 0.1% Tween-20) and 100 mM dithiothreitol (DTT; Sigma-Aldrich 3860-OP) were prepared fresh. RNA samples (50 ul) were heated to 65ºC for 5 minutes and iced. Resuspended µMass beads (100 µl) were added and samples were incubated for 15 minutes in the dark at room temperature with rotation. µMacs columns were equilibrated with 2 x 100 µl of nucleic acid buffer (supplied with kit) before applying the RNA-bead samples to the columns. Columns were washed with twice with 65ºC MPG buffer and twice with room temperature buffer. TU-tagged RNA was eluted from each column with 2 x 100 µl 100 mM DTT heated to 65 ºC. Eluted RNA was recovered by NaOAc - ethanol precipitation as above, resulting in two biological samples of hair cell enriched, TU-tagged RNA from *Tg(UPRT)* larvae treated with 4TU and two biological samples of tagged RNA from non-transgenic larvae treated with 4sU.

RNA-seq library construction and sequencing was done by the OHSU Massively Parallel Sequencing Shared Resource (Oregon Health & Science University, Portland OR). The raw RNA-seq data was imported into an OHSU instance of the Galaxy platform [34] and mapped to the *Danio rerio* GRCz10 genome. The resulting BAM files were imported to SeqMonk (https://www.bioinformatics.babraham.ac.uk/projects/seqmonk/) for data visualization and statistical analysis using default parameters for DESeq2. Transcripts that were significantly enriched in the *Tg(UPRT)* samples were analyzed for GO biological process term enrichment using the Panther database [35,36]. Looking for other possible microtubule-associated genes, we also manually annotated the enriched genes which did not have GO annotation by searching PubMed for "('*root gene symbol*') AND (microtubule OR cilium OR cilia OR flagella OR axoneme)". Analysis of *ODF3L2* and *SAXO2* genomic positions relative to known deafness loci was done using information from the Hereditary Hearing Loss website [37] and by searching the GRCh38.p13 human genome assembly

through Ensembl [38] for the loci-defining genetic markers described in the relevant publications (Table 1).

2.4. Whole mount mRNA in situ hybridization

mRNA in situ hybridizations (ISH) for *ankef1a*, *odf3l2a,* and *saxo2* were performed as described [32]. Probe templates were amplified using primers listed in Table S1. The *odf3l2a* template was amplified from total RNA with T3 and T7 sites on the forward and reverse primers respectively and the DIG-labeled antisense probe was synthesized directly from purified PCR product using T7 RNA polymerase (NEB M0251S). The *ankef1a* and *saxo2* probe templates were amplified from total RNA with gene specific primers and cloned into the pCR4-TOPO vector (Thermo Fisher 450071). DIG-labeled antisense probes for *ankef1a* and *saxo2* were synthesized with the appropriate RNA polymerase from linearized plasmids (*ankef1a*: NotI, T3 (M0378S); *saxo2*: PmeI, T7). Note that our *ankef1a* probe encompasses the entire open reading frame (2340 bp), with 613 bp at its 3' end overlapping with the previously published *ankef1a* probe [39].

2.5. Confocal microscopy, image analysis, and statistics

Live zebrafish larvae (5-7 dpf) were anesthetized in 0.016% MS-222 and mounted in 1.2% low-melting point agarose overlaid with E3 media containing MS-222. Confocal imaging was performed with a Zeiss LSM 700 confocal microscope equipped with a 40X water immersion objective. To image inner ear sensory patches, optical slices were acquired every 0.6-0.7 µm for a depth of 22-32 µm. For clarity's sake, projections were made from a contiguous subset of the complete stack, typically representing a depth of 7-20 µm. Neuromasts D1, MI1, O1, or SO2 were imaged. Because fluorescence intensity levels differed between the various transgenic lines, gain settings were tailored for each transgene. In particular, the *saxo2-mKate2* "severe" line was imaged at lower gain settings to avoid overexposing the intensely bright mKate2 puncta. Pixel intensity and kinocilium length analyses were done in Fiji [40] and the "cool" lookup table was used to encode pixel intensity in maximum Z-projections. Neuromast images in Figure 2E-H contain "choppiness" artifacts produced by rotation of 3D Z-projections. Images were compiled and adjusted for brightness and contrast in Adobe Photoshop CC.

Length measurements for lateral cristae kinocilia were done by tracing a kinocilium from base to tip through a confocal Z-stack using the SNT plugin for ImageJ [41,42] and calculating the Euclidean distance for kinocilial length by Pythagorean theorem. The transmitted light channel was used to define the start and end of each kinocilium. A single biological sample (n) is defined as the per larva average of the five tallest kinocilia that could be unambiguously traced. Per larva averages were used for statistical comparisons between transgenic larvae and non-transgenic siblings.

Fluorescent protein distributions along the length of lateral crista kinocilia were quantified in ImageJ using the "plot profile" function with a segmented line width setting of "2". 16-bit pixel intensity values were recorded every 0.064 µm. Measurable kinocilia were defined as having a minimum length of 32 µm and for which the intensity profile could be unambiguously measured from base to distal tip using the transmitted light channel as a guide. To account for differences in kinocilial length, pixel intensity values were registered to the most distal measurement of each kinocilium, meaning that proximal intensity values for kinocilia that are longer than 32 µm are not included in the intensity profile measurement

analysis. Pixel intensity values at each position were averaged from all measured kinocilia to create an average gray value over a distance of 32 µm. To account for differences in overall fluorescence levels between transgenes, the average gray values were rescaled using min-max normalization to a 0-100 scale and plotted as log2 values fit with a loess curve.

RNA sequencing data were visualized and plotted using Seqmonk (https://www.bioinformatics.babraham.ac.uk/projects/seqmonk/) and analyzed using default Seqmonk settings for DESeq2. Statistical tests for kinocilial length were performed in R Studio [43] using the base R stats package [44] for Welch two-sided t-tests and the ANOVA. Plots were generated with ggplot2 [45].

3. Results

3.1. Identification of putative kinocilia-associated, hair cell-enriched transcripts.

Thiouracil (TU) tagging is a method for purifying mRNA transcripts from specific cell types [46]. To identify genes expressed in sensory hair cells (Figure 1A), we performed TU-tagged RNA-seq experiments on larval zebrafish, introducing several protocol changes relative to our previous study (See Methods) [32]. We identified 1838 features that were significantly enriched in the 4TU-treated *Tg(UPRT)* sample vs. the 4sU-treated wild type controls (Figure 1B). See Table S2 for the full list of significantly TU-enriched genes from

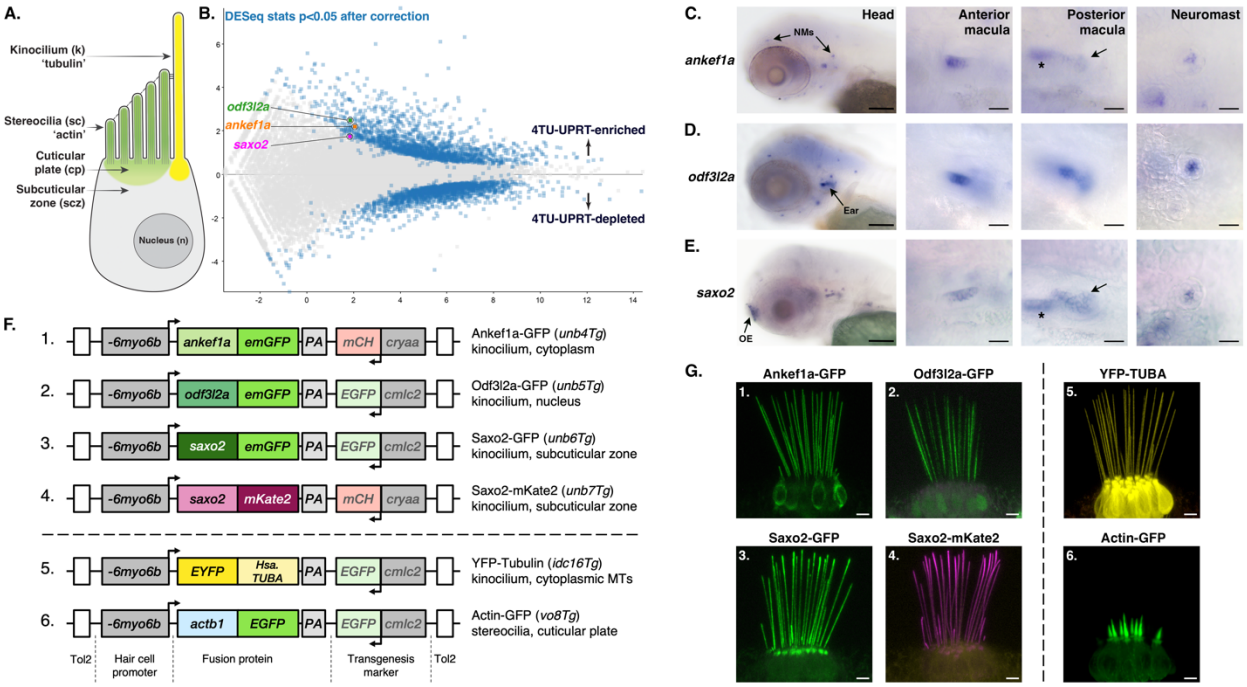

Figure 1. Identification of cilium-associated genes with enriched expression in zebrafish hair cells. **A.** Diagram of a generic sensory hair cell. **B.** Scatter plot of differentially expressed genes identified by TU-tagging. *ankef1a*, *odf3l2a*, and *saxo2* are indicated in the 4TU-UPRT-enriched population. **C-E.** mRNA in situ hybridization (ISH) for *ankef1a*, *odf3l2a* and *saxo2* in 3 days post-fertilization (dpf) zebrafish larvae. NMs = neuromasts; OE = olfactory epithelium. In the *ankef1a* and *saxo2* posterior macula panels, arrows point to the posterior macula sensory patch while the asterisk indicates the out of focus anterior macula. **F.** Schematic of transgenic genes used in this study. **G.** Overview of Ankef1a-GFP (1), Odf3l2a-GFP (2), Saxo2-GFP (3), Saxo2-mKate2 (4), YFP-TUBA (5), and Actb1-GFP (6) protein localization in the lateral cristae of larval zebrafish at 5-6 dpf. Scale bars are 100 µm for the head shots in C-E, 20 µm for all other ISH panels. Scale bars are 5 µm in G.

this study. Gene Ontology (GO) enrichment analysis of 1675 uniquely mapped features reveals that genes associated with hearing, hair cells, and inner ear development are statistically overrepresented in the TU-enriched dataset (Table S3), confirming that the experiment successfully enriched for hair cell transcripts. There is also a significant enrichment of genes associated with microtubule-and cilium-based processes (Table S4), highlighting genes with potential roles in the structure and / or function of kinocilia.

Next, we manually searched the entire TU-enriched dataset for putative kinocilial genes that may be associated with deafness phenotypes in mice and humans, but whose protein products have not been previously localized to the kinocilium. For this study, we focus on three such genes - *ankef1a*, *odf3l2a*, and *saxo2*. Enriched hair cell expression for all three genes was confirmed by mRNA in situ hybridization on 3 days post-fertilization (dpf) larvae. *ankef1a* is primarily expressed in inner ear and lateral line hair cells (Figure 1C). This restricted pattern differs from a previous study where *ankef1a* was shown to be more broadly expressed [39]. Using a similar probe as the earlier study against the 3' end of the transcript results in a comparably broad expression pattern (Figure S1). *odf3l2a* expression is restricted to inner ear and lateral line hair cells (Figure 1D), consistent with the pattern reported for the *et10.4* enhancer trap line where the transgenic insertion is 1.5 kilobases (kb) upstream of the *odf3l2a* gene [47]. *saxo2* is also expressed in otic and lateral line hair cells, with additional expression in the developing olfactory epithelia (Figure 1E).

3.2. Evaluation of ANKEF1, ODF3L2, and SAXO2 as potential human deafness genes.

Ankyrin repeat and EF-hand domain containing 1 (ANKEF1) is predicted to contain protein-protein interaction (ankyrin) and calcium-sensing/binding (EF-hand) domains. Functionally, *Ankef1* has been implicated in *Xenopus* gastrulation and fertility in male mice [48,49]. ANKEF1 protein localization to the cilium has not been demonstrated, but transcriptomic and proteomic analyses suggest it is enriched in ciliated cells (including mouse and zebrafish hair cells) [39,50–57].

Human *ANKEF1* is on chromosome 20 (GRCh38: 20:10034987-10058303) and not located near any known human deafness loci [37] (Table 1). However, the mouse *Ankef1* ortholog is located within the coloboma (*Cm*) deletion locus [58,59]. *Cm* heterozygotes exhibit morphological abnormalities in the organ of Corti and head bobbing indicative of vestibular defects [27,60]. Most of these *Cm* phenotypes can be attributed to the heterozygous loss of the Notch ligand Jagged 1 (*Jag1*). However, the authors note that the *Cm* and *Jag1* mutant phenotypes are not equivalent and speculate that other genes within deletion may contribute to the inner ear defects in *Cm* mutants [27].

Outer dense fiber protein 3-like 2 (ODF3L2) is a member of the ODF3 family of proteins which are characterized by sperm-tail PG (proline-glycine)-rich (STPGR) repeat domains. Note that although ODF families 1-4 share a common nomenclature and associate with microtubule-based structures, these four ODF families are not evolutionarily related to one another. ODF3 (SHIPPO1) was first identified as a component of the outer dense fibers (ODFs) of mouse sperm tails [61]. However, *Odf3* family genes are also expressed in ciliated cells that lack outer dense fibers [62–65], suggesting a broader role in microtubule-based structures [66]. Consistent with this idea, an Odf3l2 homolog in *Giardia* forms part of the basal body proteome [67], human ODF3L2 can localize to cytoplasmic microtubules in a heterologous expression system [68], and *Tetrahymena* ODF3L homologs bind to axonemal microtubules [69]. However, ODF3L2 localization to the cilium has not been demonstrated.

Functionally, little is known about ODF3 and ODF3L proteins in any cell type. Zebrafish *odf3l2a* is a hair cell-enriched transcript [57] and, although evidence for *Odf3l2* expression in mammalian hair cells is weak, *Odf3l2* knockout mice display high frequency hearing loss and vestibular dysfunction [70]. The underlying cellular causes for these phenotypes are unknown.

Table 1: Human *ANKEF1*, *ODF3L2*, and *SAXO2* chromosomal locations compared to potential associated deafness loci.

Human gene	Cytogenetic Location	GRCh38.p13 coordinates	Proposed deafness locus	Critical region markers	Locus coordinates	Causative gene	Reference
ANKEF1	20p12.2	20:10034987-10058303	n/a	n/a	n/a	n/a	n/a
ODF3L2	19p13.3	19:463346-474880	*DFNB72*	D19S216 - D19S1034	19:4949401-6113471	*GIPC3*	Ain et al. [71]
			DFNA57	D19S912 - D19S212	19:7806762 - 18232460	unknown	Bönsch et al. [72]
SAXO2	15q25.2	15:82262818-82284927	*DFNA30*	D15S151 - D15S130	15:87053920-94168232	unknown	Mangino et al. [73]

Human *ODF3L2* is located on chromosome 19p13.3 (GRCh38:19:463346-474880) (Table 1). The 19p13 region is home to several hearing loss loci, including *DFNB15*/*72*/*95* (*GIPC3*) [74,75], *DFNB68* (*S1PR2*) [76], *DFNB81* / Perrault syndrome (*CLPP*) [74,77], as well as the autosomal dominant *DNFA57* locus (gene unknown) [72]. The *DFNB72* critical region was mapped between markers D19S216 and D19S1034 (GRCh38:19:4949401-6113471) [71]. Although the Shared Harvard Inner-Ear Database (SHIELD) [28] reports that *ODF3L2* is located within the *DFNB72* critical region, the GRCh38 human genome assembly places *ODF3L2* at least 4.4 MB away from the closest *DFNB72* marker D19S216. The *DFNA57* critical region was mapped between markers D19S912 and D19S212 (GRCh38:19:7806762:18232460). *ODF3L2* is almost 7 MB away from the closest marker D19S592 and over 9 MB away from the maximum LOD score marker D19S586. However, the telomeric boundary was defined from a single patient and the authors acknowledge an unlikely possibility that the *DFNA57* interval extends to the telomere. If this is the case, *ODF3L2* remains as a candidate gene for *DFNA57*.

Stabilizer of axonemal microtubules 2 (SAXO2 / FAM154B) is the second of two SAXO family members that are part of the microtubule associated protein 6 (MAP6) family [78,79]. SAXO proteins can stabilize microtubules and use their "Mn" repeat domains to associate with basal bodies, centrioles, and cilia [79–82]. Interestingly, SAXO and MAP6 are MIPs (microtubule inner proteins), meaning they reside in the luminal space of microtubules [83–86]. Furthermore, luminal MAP6 can stabilize microtubule curvature [87], though it is unknown whether SAXO proteins also share this functionality. *Saxo2* is enriched in hair cell transcriptomic datasets from mice and zebrafish [55,57,88] but has not been functionally characterized.

Human *SAXO2* is located on 15q25.2 (Table 1), near several sensorineural deafness loci including *DFNA30* (gene unknown) [73], *DFNA68* (*HOMER*) [89,90], *DFNB48* (*CIB2*) [91,92], and *OTSC1* [93]. SHIELD reports that *SAXO2* maps to the *DFNA30* locus. The

critical region for *DFNA30* lies between markers D15S151 and D15S130 (GRCh38:15:87053920-94168232) with a maximum LOD score for marker D15S1004 [73]. However, current genomic coordinates for *SAXO2* (GRCh38:15:82262818-82284927) place it outside the *DFNA30* critical interval, 4.8 MB away from the closest marker D15S151 and 11.5 MB away from D15S1004.

3.3. Distinct localization patterns of Ankef1a, Odf3l2a, and Saxo2 in the kinocilium.

To analyze the subcellular localization of Ankef1a, Odf3l2a, and Saxo2 in zebrafish hair cells, we created stable transgenic fish expressing fluorescently-tagged versions of these proteins under control of the hair cell-specific *myo6b* promoter (Figure 1F). Like YFP-Tubulin, tagged Ankef1a, Odf3l2a, and Saxo2 proteins all exhibit robust localization to the kinocilium (Figure 1G). By comparison, EGFP alone is largely restricted to the cytoplasm and nucleoplasm, with faint signal in the kinocilia (Figure S2).

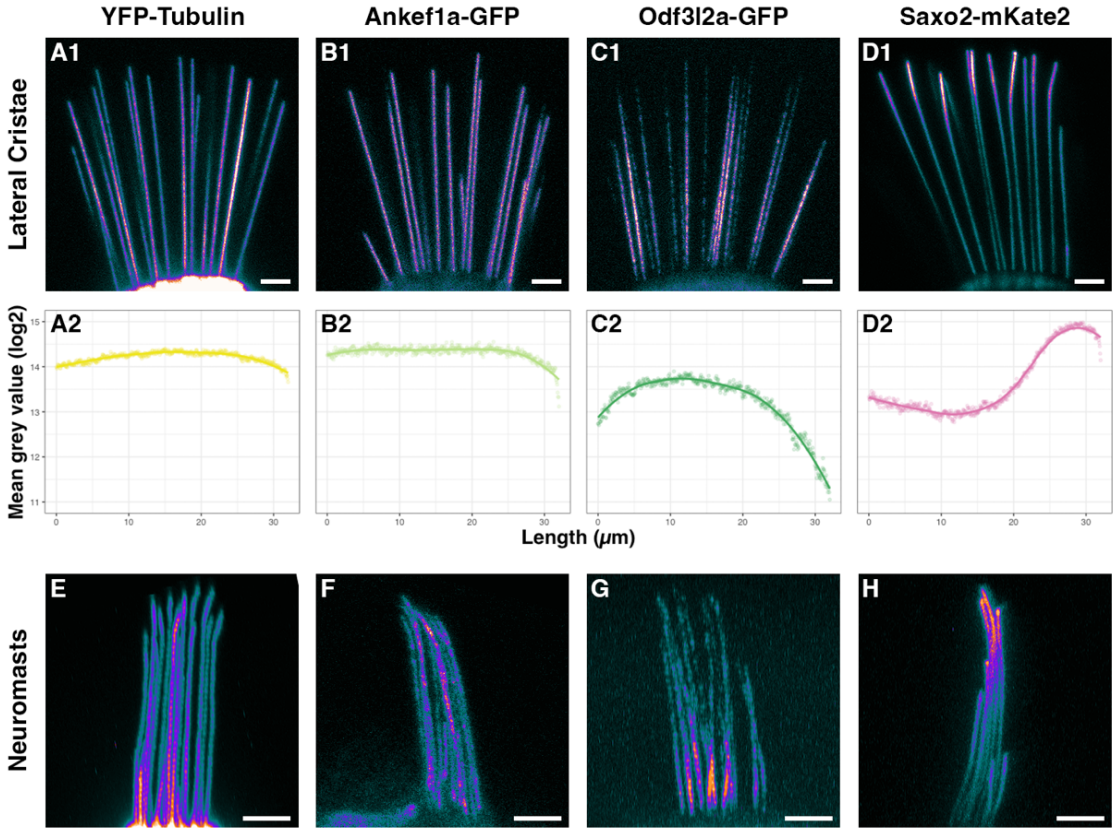

Figure 2. Distributions of tubulin, Ankef1a, Odf3l2a, and Saxo2 in the hair cell kinocilium at 5-6 days post-fertilization. **A1 – D1.** Pixel intensity-encoded images of tagged alpha tubulin, Ankef1a, Odf3l2a, and Saxo2 proteins in the kinocilia of lateral cristae hair cells. Brighter colours indicate higher fluorescence intensity. **A2 – D2.** Scatter plots of averaged mean grey values (log2) for fluorescence intensity from kinocilia in the lateral cristae of YFP-TUBA (n = 35 kinocilia from 8 individuals), Ankef1a-GFP (n = 23 from 8 individuals), Odf3l2a-GFP (n = 30 from 11 individuals), and Saxo2-mKate2 (n = 17 from 6 individuals). Position 0 µm is from the proximal region near the base of kinocilia and position 32 µm is the distal-most tip. **E – H.** Pixel intensity-encoded images of neuromast kinocilia from YFP-TUBA, Ankef1a-GFP, Odf3l2a-GFP, and Saxo2-mKate2 expressing zebrafish larvae. Scale bars are 5 µm in panels A1-D1, E-H.

We imaged the lateral cristae and neuromasts of live larvae at 5-6 dpf and encoded differences in pixel intensity by applying the ImageJ "cool" lookup table to maximum z-projections (Figure 2A1-D1, E-H). We also quantified fluorescence intensity in these kinocilia and present the average fluorescence intensity distribution as a log2 mean grey value over the most distal 32 µm (Figure 2A2-D2). For comparison, we also used the *Tg(myo6b:yfp-Hsa.TUBA)idc16* line that expresses YFP-tagged alpha tubulin in hair cells, marking both cytoplasmic and axonemal microtubules as well as a pool of unpolymerized tubulin. As expected, YFP-TUBA is uniformly distributed along the length of the hair cell kinocilium in the lateral cristae and neuromasts (Figure 2A1, A2, E). Ankef1a-GFP displays a similarly uniform distribution from base to tip (Figure 2B1, B2, F). The distribution of Odf3l2a-GFP is distinct from that of tubulin and Ankef1a, with Odf3l2a being more restricted to the middle-proximal region of the kinocilium (Figure 2C1, C2, G). The distribution of Saxo2-mKate2 is complementary to that of Odf3l2a, with enriched localization to the distal region of the kinocilium and a depletion in the middle-proximal zone (Figure 2D1, D2, H). Interestingly, we observe bent kinocilia in the lateral cristae of Saxo2-mKate2 transgenics (Figure 2D1), a phenotype we do not observe in the other transgenic lines or in non-transgenic siblings. Saxo2-GFP is also enriched in the distal region (Figure S3A, B), but we do not observe kinocilial curvature in this line. All five tagged proteins also show similarly distinct localization patterns in hair cells of the anterior macula (Figure S4). Together, these transgenes demonstrate that Ankef1a, Odf3l2a, and Saxo2 are cilia-associated proteins and suggest that each one exhibits a distinct distribution pattern in the kinocilia of zebrafish hair cells.

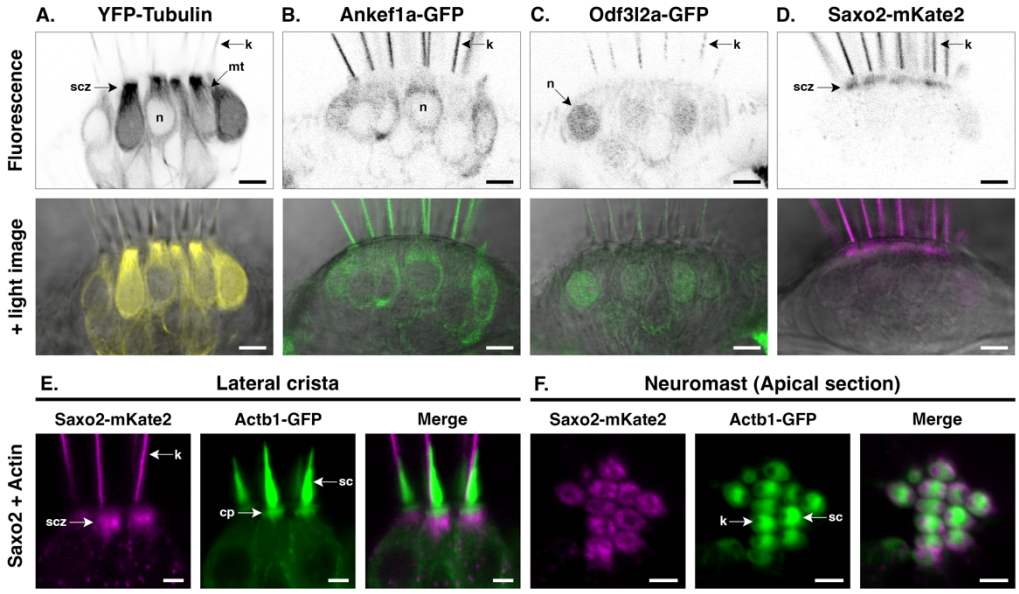

Figure 3. Distinct protein localization patterns in the hair cell soma. **A – D.** Details of YFP-TUBA, Ankef1a-GFP, Odf3l2a-GFP, and Saxo2-mKate2 in the hair cell body at 5-6 days post-fertilization. Top panels are black and white representations of the fluorescence channel and lower panels are fluorescence with the corresponding light image. **E, F.** Saxo2-mKate2 (magenta) accumulations in apical part of the hair cell body in cristae and neuromasts. GFP-tagged beta actin is shown in green. scz = subcuticular zone; mt = microtubule; k = kinocilium; n = nucleus; cp = cuticular plate; sc = stereocilia. Scale bars are 5 µm in A – D and 2.5 µm in E and F.

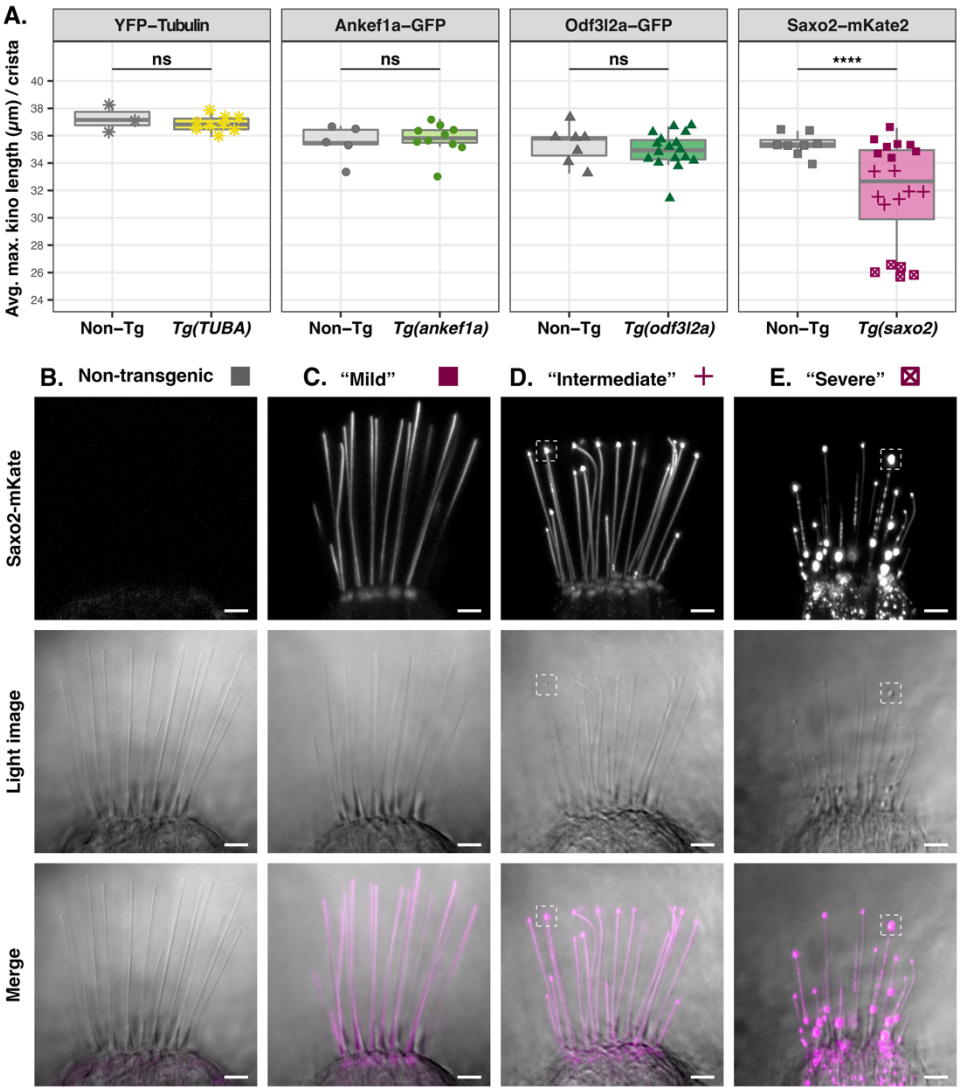

Figure 4. Effect of tubulin, Ankef1a, Odf3l2a, and Saxo2 overexpression on kinocilial length and morphology at 5-6 days post-fertilization. **A.** Boxplots of maximum kinocilia length in the lateral crista of *YFP-TUBA*, *ankef1a-GFP*, *odf3l2a-GFP*, and *saxo2-mKate2* transgenics and their non-transgenic siblings. Data points are the average length of the five tallest kinocilia from an individual larva. Based on the morphological phenotypes of the three Saxo2-mKate2 transgenic lines, these data points are grouped as "mild" (solid squares), "intermediate" (crosses), and "severe" (boxed x's). Two-tailed Welch's t-test statistics - YFP-tubulin (6 dpf): non-Tg, n = 3 larvae, mean = 37.3 µm; *Tg(TUBA)*, n = 9, mean = 36.9 µm; t = 0.67757, df = 2.5116, p = 0.5551. Ankef1a-GFP (5 dpf): non-Tg, n = 5, mean = 35.5 µm; *Tg(ankef1a)*, n = 10, mean = 35.7 µm; t = 0.41384, df = 7.079, p = 0.6912. Odf3l2a-GFP (5 dpf): non-Tg, n = 7, mean = 35.3 µm; *Tg(odf3l2a)*, n = 17, mean = 35.0 µm; t = 0.5913, df = 10.931, p = 0.5663. Saxo2-mKate2 (5 dpf) one-way ANOVA ($F_{3,24}$ = 193.3, p < 2e-16). See text for results of pairwise comparisons between the Saxo2-mKate2 phenotypes. **B - E.** Representative images of lateral cristae from non-transgenic (B) and *saxo2-mKate2* transgenics categorized as "mild" (C), "intermediate" (D), and "severe" (E). The dashed boxes in D and E highlight examples of the "bulbed" kinocilial phenotype. ns = not significant; **** = p < 0.00001. Scale bars are 5 µm.

3.4. Ankef1a, Odf3l2a, and Saxo2 exhibit distinct localization patterns in the hair cell soma that differ from cytoplasmic tubulin.

To determine if Ankef1a, Odf3l2a, and Saxo2 also associate with cytoplasmic tubulin, we compared the cytoplasmic distributions of these tagged proteins to that of YFP-TUBA in the soma of hair cells in the lateral cristae and neuromasts (Figures 3 and S5). In the cytoplasm, the YFP-TUBA signal is strongest in the apical subcuticular zone that lies just below the actin-rich cuticular plate. Cytoplasmic microtubules are also evident (Figure 3A). Ankef1a-GFP is largely excluded from the subcuticular zone and there is no obvious association with cytoplasmic microtubules (Figure 3B). Instead, the Ankef1a-GFP signal is diffuse throughout the perinuclear cytoplasm. In contrast to Ankef1a, Odf3l2a-GFP signal is mostly absent from the cytoplasm, instead accumulating in the nucleus of some hair cells. In neuromasts, Ankef1a and Odf3l2a display similar localization patterns as in cristae (Figure S5A, B). Lastly, Saxo2-mKate2 does not associate with cytoplasmic microtubules but instead accumulates in the subcuticular zone beneath the cuticular plate, marked here by GFP-tagged beta actin (Figure 3D-F). YFP-TUBA also accumulates in this region (Figure S6A). Likewise, Saxo2-GFP displays a similar apical accumulation in the cell body (Figures 1G, S3A). In top-down views of neuromast hair cells, both Saxo2-mKate2 (Figure 3F) and Saxo2-GFP (Figure S5C) accumulate in ring-like structures surrounding the cuticular plate. In summary, although Ankef1a, Odf3l2a, and Saxo2 all localize with tubulin in the kinocilium, none of these proteins share the same distribution pattern as YFP-TUBA in the hair cell soma, nor do their patterns overlap with one another.

3.5. Saxo2-mKate2 overexpression results in curved, truncated, and 'bulbed' kinocilia.

Next, we measured kinocilial height in the lateral crista to determine whether overexpression of Ankef1a, Odf3l2a, or Saxo2 influences kinocilial morphology. The average maximum heights of kinocilia in *YFP-TUBA*, *ankef1a-GFP*, and *odf3l2a-GFP* transgenics were statistically indistinguishable from their non-transgenic siblings (Figure 4A). In contrast to these single transgenic lines, we identified at least three independent lines for *saxo2-mKate2* with different levels of expression (Figure S7) which we categorized as "mild", "intermediate", and "severe" in terms of their kinocilial phenotypes (Figure 4B-E). A one-way ANOVA comparing the three *saxo2-mKate2* phenotypes and non-transgenic siblings reveals significant differences in kinocilial length ($F_{3,24} = 193.3$, $p < 2e\text{-}16$). Compared to non-transgenic siblings, maximum height is not affected in "mild" *saxo2-mKate2* transgenics, despite examples of curved kinocilia (Figure 4A-C; non-Tg, $n = 8$, mean = 35.4 µm; "mild", $n = 8$, mean = 35.3 µm; padj = 0.9858). However, both the "intermediate" and "severe" phenotypes have significantly shorter kinocilia compared to non-transgenic siblings (Figure 4A, D, E; "intermediate", $n = 7$ mean = 32.1 µm, padj < 0.0001; "severe", $n = 5$, mean = 26.1 µm, padj < 0.0001). Transgenics with the "intermediate" phenotype exhibit kinocilial curvature and bulbed tips marked by an accumulation of Saxo2-mKate2 (Figure 4D). Lastly, the "severe" Saxo2-mKate2 overexpression phenotype includes a further reduction in average maximum kinocilia height and increased prominence of bulbed tips (Figure 4E). The severe phenotype is also marked by a punctate accumulation of Saxo2-mKate2 in the cell bodies and along the kinocilia. Some of these puncta are bidirectionally mobile in the kinocilia (Video S1). Neuromasts from the severely affected larvae display a similar phenotype of truncated kinocilia (Figure S8). Surprisingly, these "severe" *saxo2-mKate2* transgenics are viable and qualitatively do not

exhibit obvious auditory or vestibular phenotypes as larvae or adults. The Saxo2-GFP line does not exhibit curved kinocilia nor a significant change in kinocilial height (t = -1.8712, df = 5.5674, p-value = 0.1143) (Figure S3C). In summary, transgenic expression of GFP-tagged Ankef1a, Odf3l2a, and Saxo2 does not affect kinocilial height. This is also true of the Saxo2-mKate2 line with lower levels of expression though curved kinocilia are common. Transgenic lines with elevated Saxo2-mKate2 have bulbed and truncated kinocilia.

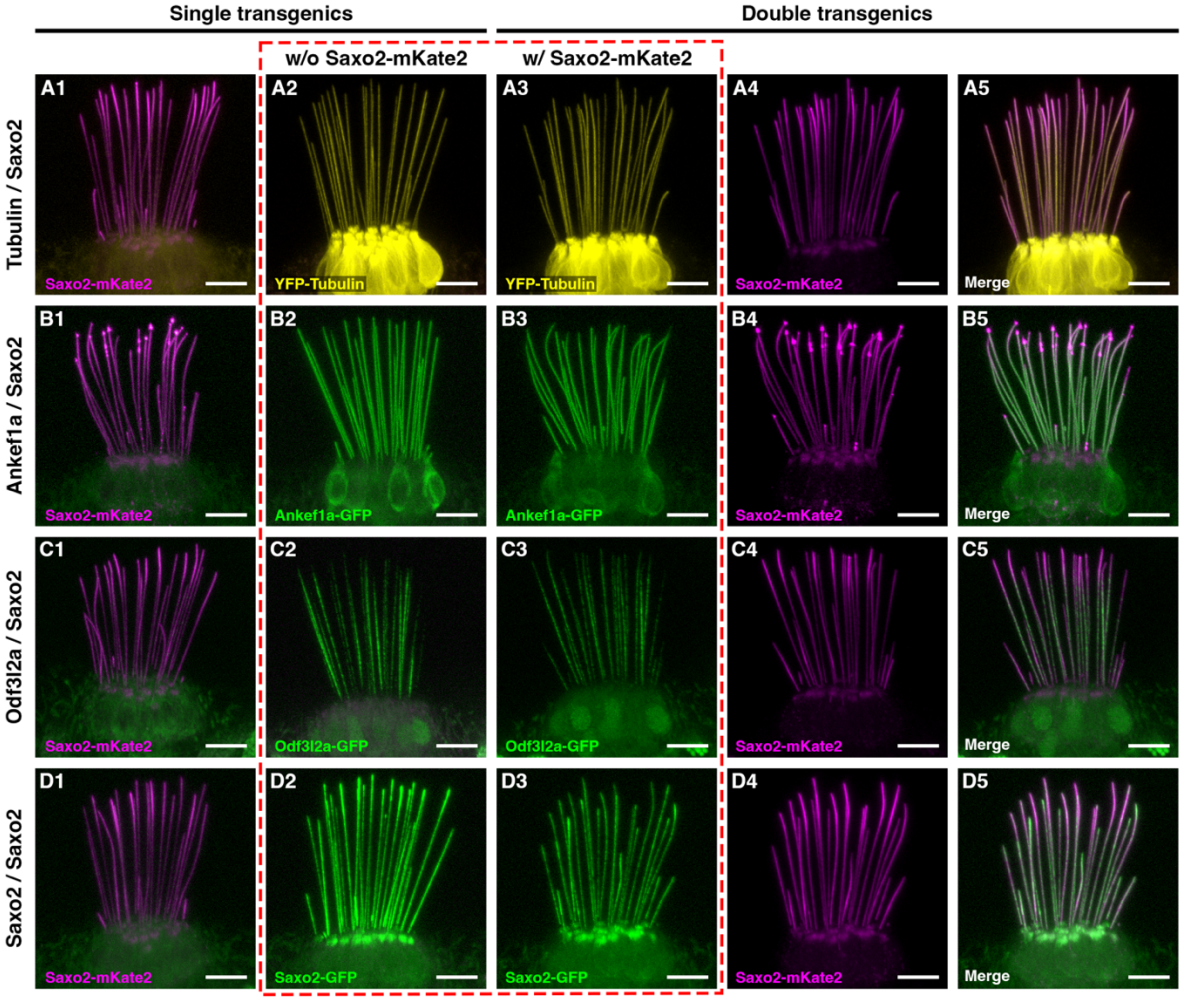

Figure 5. Co-expression of Saxo2-mKate2 with YFP-tubulin (**A**), Ankef1a-GFP (**B**), Odf3l2a-GFP (**C**), and Saxo2-GFP (**D**) at 5-6 days post-fertilization. Column 1 and 2 of each row shows single transgenic siblings while columns 3 and 4 show individual channels from a double transgenic larva. Column 5 shows the merged channels from columns 3 and 4. The dashed red box compares YFP-TUBA, Ankef1a-GFP, Odf3l2a-GFP, and Saxo2-GFP localization without (A2-D2) or with (A3-D3) the presence of Saxo2-mKate2. Scale bars are 5 µm in all panels.

3.6. Ankef1a, Odf3l2a, and tubulin distribution patterns are not influenced by Saxo2.

Given that Saxo2-mKate2 can alter kinocilial morphology, we next tested whether the presence of Saxo2-mKate2 influences the distributions of YFP-TUBA, Ankef1a-GFP, Odf3l2a-GFP, and Saxo2-GFP. We produced four combinations of double transgenic fish,

each with Saxo2-mKate2 as a common factor. Co-expression of Saxo2-mKate2 with YFP-TUBA (Figure 5A1-5, Figure S6), Ankef1a-GFP (Figure 5B1-5), or Odf3l2a-GFP (Figure 5C1-5) did not alter the distribution patterns of either pair of proteins relative to single transgenic siblings. An example of the Saxo2-mKate2 "intermediate" phenotype is shown in panels B1, B3-5 while the "mild" phenotype is shown in the other examples. On the other hand, rather than simply overlap with one another, co-expression of Saxo2-mKate and Saxo2-GFP reveals a form of competition for space between these two transgenic proteins (Figure 5D1-5). Most obviously at the tips, either the mKate2 or GFP version of Saxo2 is more abundant with Saxo2-mKate2 appearing to outcompete Saxo2-GFP at the tips of most kinocilia. Taken together, these data suggest that Saxo2 does not positively or negatively influence the distributions of tubulin, Ankef1a, or Odf3l2a in the kinocilium.

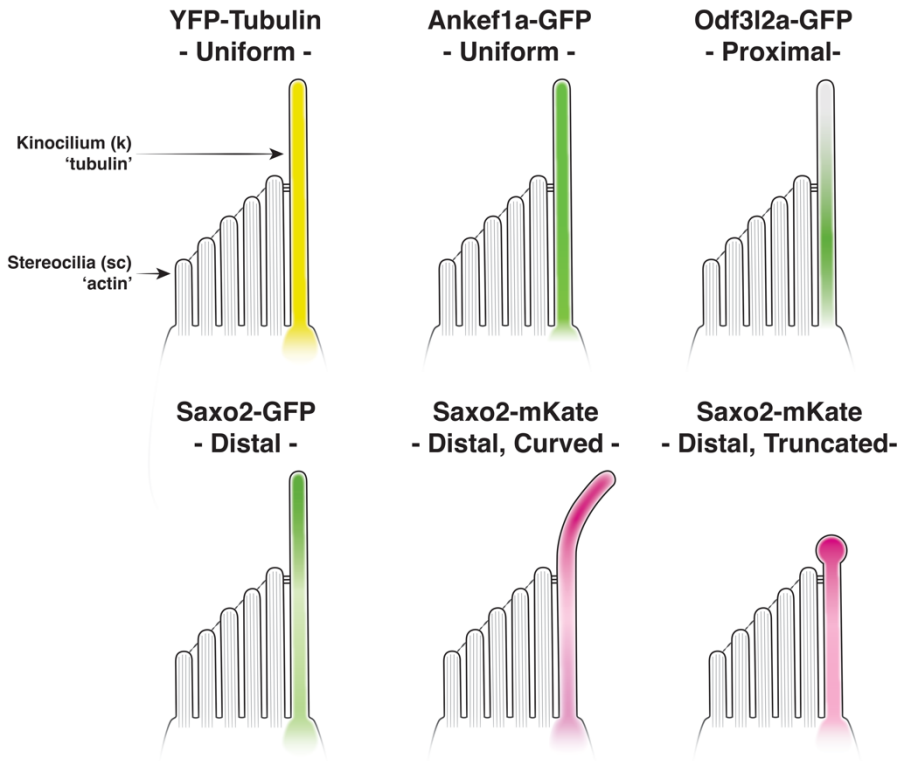

Figure 6. Summary of kinocilial localization patterns and phenotypes for Ankef1a, Odf3l2a, and Saxo2 transgenic proteins compared to tubulin.

4. Discussion

4.1. Utility of TU-tagging to identify hair cell transcripts.

As with our previously published work [32], here we show that hair cell-enriched transcripts can be identified by thiouracil tagging of newly synthesized RNA. GO analysis confirms that hair cell transcripts are overrepresented in the TU-tagged samples. We also identified all of the TU-enriched transcripts from our previously report, although some gene identifiers from GRCz10 are no longer part of the current GRCz11 genome assembly (*fam188b2* ENSDARG00000069867, *stereocilin-like* genes ENSDARG00000078845 and

ENSDARG00000088059, and uncharacterized gene ENSDARG00000088304). Changes to the experimental protocol greatly increased the number of significantly enriched genes in the TU-tagged samples. However, in addition to an enrichment of genes related to hair cells and cilia, this dataset is also enriched for genes involved in electron transport and ATP synthesis, iron metabolism, and visual system development and function (Table S2). These results confirm the signal-to-noise problem that seems inherent to TU-tagging in zebrafish. Unless one's experiment requires time resolved differentiation between nascent and preexisting pools of RNA, recent advances in single cell RNA sequencing have largely rendered more error-prone techniques like TU-tagging obsolete.

4.2. Determining the subcellular localization for putative kinocilial proteins.

GFP-tagged proteins have long been valuable tools for live imaging of protein localization [94,95]. This technique has proven particularly invaluable in the analysis of protein localization and function in zebrafish hair cells [8,31,96–104]. GFP-tagging has also been used extensively to assay for protein localization to microtubules and cilia [68,105–108], including in hair cells [109]. MAP6 family members have also been studied in cultured cells and in vitro using fluorescent protein tags, including MAP6-GFP [87,110,111], and SAXO1- and SAXO2-GFP [80,81]. Importantly, the GFP-tag does not seem to interfere with normal function or localization of cilia-associated proteins. MAP6-GFP and endogenous MAP6 display similar enrichment in the proximal part of neuronal axons [112], and GFP-tagged versions of the Eps15 homology domain proteins EHD1 and EHD3 exhibit the same restricted localization to the proximal part of the primary cilium as the endogenous protein [113]. Thus, GFP-tagging of cilial proteins is a powerful tool for analyzing protein localization in live cells.

4.3. Regionalization of the hair cell kinocilium.

Primary cilia are compartmentalized along their proximal-distal axis into functional domains marked by distinct protein compositions [114,115]. However, regionalization of the hair cell kinocilium has received little attention. Here, we express tagged versions of hair cell-enriched proteins Ankef1a, Odf3l2a, and Saxo2 in zebrafish to demonstrate their localization to the kinocilium of hair cells. Live imaging of these transgenic proteins also reveals their unique kinocilial localization patterns (Figures 1 and 2, summarized in Figure 6). Like YFP-tagged tubulin, Ankef1a-GFP is uniformly distributed along the entire length of the kinocilium. Interestingly, Odf3l2a and Saxo2 exhibit somewhat complementary localization patterns, with Odf3l2a being restricted to the proximal-middle region and Saxo2 accumulating at the kinocilial tips. Together, our study is the first to demonstrate cilial localization for these proteins in hair cells and lends support to the idea that the kinocilium is compartmentalized along its proximal-distal axis. It remains to be tested whether these domains are important for kinocilial structure and the sensory function of hair cells.

Based on our results, we propose that Ankef1a, Odf3l2a, and Saxo2 represent three examples of proteins with distinct kinocilial localization or retention signals. Analogous to how tubulin monomers line up in an orderly fashion, Ankef1a may contain a "queue-up" motif that prevents accumulation once all available spots are filled, assuring an uniform distribution of Ankef1a along the axoneme. Odf3l2a may encode a "stop" signal that restricts localization to the middle-proximal compartment. Lastly, Saxo2 may contain a "keep walking" signal that allows the protein to accumulate at the plus ends of the axonemal microtubules. These putative localization or sorting motifs may interact with subunits of the

intraflagellar transport (IFT) machinery and / or with components of the transition zone or axoneme to produce these three distinct kinocilial localization patterns. Our results lay the foundation for future structure-function experiments to understand how these proteins are targeted to cilia and, together with loss-of-function models, to characterize their functional domains.

4.4. Saxo2 promotes formation of curved and truncated kinocilia.

Kinocilial length and morphology are normal in our *ankef1a* and *odf3l2a* transgenics. However, we find that Saxo2-mKate2 overexpression promotes the formation of curved kinocilia. SAXO proteins are members of the microtubule associated protein 6 (MAP6) family that stabilize microtubules in axons, cilia, and flagella [79,80]. Recent work shows that MAP6 and SAXO are microtubule inner proteins (MIPs) that can localize to the intraluminal space of microtubules [83–85,87]. Full length MAP6 can bind to either the outside or inside of microtubules, and intraluminal localization requires a N-terminal cysteine-rich domain [87]. Luminal MAP6 can stabilize the formation of curved or helical microtubules, a property that externally-bound MAP6 does not possess [87]. Saxo2 also features the cysteine-rich N-terminal domain of the MAP6 family [81]. Given that only luminal MAP6 induces microtubule curvature, it is possible that overexpressed Saxo2 also uses its N-terminal domain to localize to the luminal space of the axonemal microtubules in hair cells. However, additional experiments are required to verify that the curvature we observe in the Saxo2-mKate transgenics is Saxo2-dependent and to determine whether endogenous Saxo2 is a bona fide MIP in the kinocilium. However, our TU-tagging dataset is also significantly enriched for other known MIPs [116], including cilia and flagella associated proteins (Cfap20, 45, and 52), EF-hand domain containing (Efhc) proteins 1 and 2, meiosis-specific nuclear structural 1 (Mns1), and Tektins 1-3 (Tables S2, S4). There are likely to be additional hair cell-enriched MIPs and these data indicate a role for intraluminal microtubule associated proteins in our senses of hearing and balance.

Saxo2 overexpression also promotes formation of bulbed kinocilia marked by an accumulation of Saxo2 at the tip. This distal accumulation is not accompanied with a concomitant redistribution of Ankef1a, Odf3l2a, or tubulin (Figures 5 and S6). This is unlike the kinocilial bulb of bullfrog hair cells that labels strongly for beta tubulin [117]. Thus, it is likely that the "canonical" and Saxo2-induced bulbs form by different mechanisms. We also report that Saxo2 overexpression promotes formation of truncated kinocilia and that higher levels of Saxo2 expression are correlated with more severe truncations (Figure 4). This correlation suggests that excess Saxo2 is commandeering the IFT machinery, leading to Saxo2 accumulation at the tip, possibly at the expense of other components required for normal growth of the kinocilium. However, kinocilial length is unchanged in Saxo2 transgenics with more modest levels of expression (Saxo2-mKate2 "mild" and Saxo2-GFP). Our results differ from those of Dacheux et al. who reported that SAXO1 overexpression almost doubles the length of the primary cilium in cultured RPE1 cells [80]. This discrepancy could be due to differences between the SAXO proteins and / or cell types. We also note differences between the Saxo2-GFP and Saxo2-mKate2 phenotypes. Although the tip-enriched distribution patterns are similar between the two forms, we do not observe curvature or truncation of kinocilia in the Saxo2-GFP line (Figure S3). However, as the Saxo2-mKate2 phenotype intensifies with higher expression levels, we suspect that the comparatively lower levels of Saxo2-GFP expression is the reason for the phenotypic discrepancy between the two tags. There is also reason to believe that the mKate2 version of Saxo2 is trafficked more

efficiently to the kinocilium – qualitatively, we observe a greater accumulation of Saxo2-GFP in the subcuticular zone relative to Saxo2-mKate2 and Saxo2-mKate2 tends to accumulate at the tips to the partial exclusion of Saxo2-GFP when they are co-expressed (Figure 5). Although the formation of bulbed and truncated kinocilia is likely an artifact of Saxo2 overexpression, the cellular phenotype is nonetheless interesting for its lack of a behavioural correlate. The adult viability and qualitatively normal behaviour of the severe Saxo2 phenotype suggests that a partial disruption of kinocilial morphology is tolerated under laboratory conditions. This tolerance and possible genetic redundancy may account for why hair cell-enriched kinocilial genes have not been identified in genetic screens based on specific auditory or vestibular behavioural phenotypes [118].

4.5. Evaluation of ANKEF1, ODF3L2, and SAXO2 as putative hearing loss genes.

Although we and others have identified many genes that may contribute to form and function of the hair cell kinocilium, we focused on *ankef1a*, *odf3l2a*, and *saxo2* for this study based on preliminary reports of their genetic location in relation to mouse and human deafness loci. Mouse *Ankef1* is within the coloboma (*Cm*) deletion locus, phenotypes of which include planar polarity defects in the cochlear epithelium, supernumerary hair cells, and hearing and balance defects [26,27]. Deletion of the Notch ligand gene *Jag1* is responsible for most of these hearing-related phenotypes, but phenotypical differences between *Cm* and *Jag1* heterozygotes leave open the possibility that other genes in the *Cm* locus are contributing to the phenotype. Since Ankef1a is a kinocilial protein and Notch pathway mutants display polarity defects indicative of mispositioned kinocilia [119,120], it is possible that the combined heterozygous loss of *Jag1* and *Ankef1* reveals a subtle role for ANKEF1 in kinocilial development which would not be apparent otherwise. Because ANKEF1 has protein-protein interaction Ankyrin repeats and calcium-sensing EF hand domains, one may speculate that ANKEF1 mediates protein-protein interactions in the kinocilium in response to changes in calcium concentrations.

A targeted knockout of *Odf3l2* in mice results in high frequency hearing loss and vestibular deficits [70,121,122]. The cellular basis for these phenotypes is unclear as mouse *Odf3l2* is not robustly expressed in either cochlear or vestibular hair cells [50,88,123]. However, *Odf3l2* expression is detected in outer pillar cells [123,124], suggesting a non-hair cell basis for the mutant phenotype. Interestingly, the homologous *Odf3b* is strongly expressed in mammalian hair cells, but the knockout mice do not exhibit auditory or vestibular phenotypes [122]. Zebrafish *odf3l2a* is expressed in both inner ear and lateral line hair cells (Figure 1C) [57,125] whereas *odf3b* is specifically expressed in ciliated cells of the olfactory epithelia and pronephros [126]. Zebrafish have a second ortholog (*odf3l2b*) whose expression is restricted to the testis [127]. Thus, vertebrate hair cells may utilize different *ODF3* orthologs – *ODF3B* in mammals and *odf3l2a* in fish.

Saxo2 transcripts are enriched in mouse cochlear and vestibular hair cells [50,88,123,124] as well as the inner ear and lateral line hair cells of zebrafish (Figure 1D) [57,125]. Enriched expression in the olfactory epithelia is also shared between mice and fish [107]. However, unlike *Odf3l2*, there are no published loss-of-function animal models for *Saxo2*. Human *SAXO2* (a.k.a. *FAM154B*) and *ODF3L2* were reported in SHIELD as mapping to deafness loci *DFNA30* and *DFNB72*, respectively [28]. *DFNA30* is an autosomal dominant form of nonsyndromic hearing loss for which the causative gene remains unknown [73]. However, neither *SAXO2* or *ODF3L2* reside within any known deafness loci based on

our analysis of the genetic markers used to map these and other nearby loci. Although it is still possible that ODF3L2 and SAXO2 contribute to auditory or vestibular function, we propose they should be excluded as candidates for currently known deafness loci.

4.6. Benefits and limitations of this study.

In contrast to the short primary cilium of most cell types, sensory hair cells, in particular vestibular hair cells of the semicircular canals, possess very long kinocilia. This study takes advantage of the long kinocilium in the cristae of larval zebrafish and the ability to image tagged protein localization in live animals to understand more about the sub-cellular and sub-cilial localization of these proteins. Benefits of live imaging of fluorescently tagged proteins are i) avoiding morphological distortions caused by fixation and processing, and ii) inconsistent antibody staining. Limitations include the possibility of altered protein localization patterns caused by the fluorescent protein tag or from use of a heterologous promoter to drive overexpression. However, the fact that all three proteins tested here display unique kinocilial and cytoplasmic distributions patterns suggest that these tagged proteins reflect their endogenous distribution patterns. An unexpected result from this study is Odf3l2a-GFP localization to the nucleus. Immunostaining of the endogenous protein is necessary to confirm this finding. If true, it presents the fascinating possibility of a communication channel between the kinocilia and the nucleus. Overexpression can also cause spurious phenotypes that may not be directly related to protein function. For example, the bulbed and truncated kinocilia observed in the "severe" Saxo2-mKate2 transgenic line may be an overexpression artifact caused by overloading the IFT machinery with excess Saxo2. It is also possible that the kinocilial phenotypes in the saxo2-mKate2 transgenics are artifacts of mKate expression since we do not observe similar phenotypes when Saxo2 is tagged with EGFP. However, the curved kinocilia we observe is consistent with previously reported function of MAP6-family proteins, supporting the idea that transgenically-expressed Saxo2 is stabilizing microtubule curvature in this case.

5. Conclusion

Here, we report hair cell-enriched expression of zebrafish *ankef1a*, *odf3l2a*, and *saxo2,* and show that tagged versions of these protein exhibit distinct distribution patterns within the kinocilium. Together, our results suggest that the hair cell kinocilium is regionalized along its proximal-distal axis.

Supplementary Materials: Figures S1-8, Tables S1-4, Video S1.

Author Contributions: Conceptualization, T.E.; formal analysis, T.E.; investigation, T.E., W.P.B., K.W., S.E.B., and A.V.; data curation, T.E.; writing—original draft preparation, T.E.; writing—review and editing, T.E., A.V.; visualization, T.E., S.E.B., and A.V.; supervision, T.E.; project administration, T.E.; funding acquisition, T.E. All authors have read and agreed to the published version of the manuscript.

Funding: This work was supported by funding awarded to T.E. by the Collins Medical Trust, East Carolina University's Division of Research, Economic Development and Engagement (REDE), and The Natural Science and Engineering Research Council (NSERC) of Canada Discovery Grant RGPIN-2021-0316.

Institutional Review Board Statement: All procedures involving animals were performed in accordance with animal use protocols approved at Oregon Health & Science University (2065), East Carolina University (D352), and the University of New Brunswick (22007).

Data Availability Statement: Data and code will be provided by reasonable request from a qualified researcher.

Acknowledgments: This work was conducted at three institutions (OHSU, ECU, and UNB), intermittently over approximately eight years. A special thank you to Teresa Nicolson, in whose lab at OHSU this work was initiated. Thank you also to Amy Carlos and Robert Searles of the OHSU Massively Parallel Sequencing Shared Resource for performing the RNA sequencing experiments. Many thanks to the support staff in the Nicolson lab at OHSU and to the many students who have contributed to animal care at ECU and UNB. Thank you to Christine Erickson for making the hair cell diagrams.

Conflicts of Interest: The authors declare no conflict of interest.

6. References

1. Bezares-Calderón, L.A.; Berger, J.; Jékely, G. Diversity of Cilia-Based Mechanosensory Systems and Their Functions in Marine Animal Behaviour. *Philos Trans R Soc Lond B Biol Sci* **2020**, *375*, 20190376, doi:10.1098/rstb.2019.0376.
2. Sharkova, M.; Chow, E.; Erickson, T.; Hocking, J.C. The Morphological and Functional Diversity of Apical Microvilli. *J Anat* **2022**, doi:10.1111/joa.13781.
3. Jones, C.; Roper, V.C.; Foucher, I.; Qian, D.; Banizs, B.; Petit, C.; Yoder, B.K.; Chen, P. Ciliary Proteins Link Basal Body Polarization to Planar Cell Polarity Regulation. *Nat Genet* **2008**, *40*, 69–77, doi:10.1038/ng.2007.54.
4. Moon, K.-H.; Ma, J.-H.; Min, H.; Koo, H.; Kim, H.; Ko, H.W.; Bok, J. Dysregulation of Sonic Hedgehog Signaling Causes Hearing Loss in Ciliopathy Mouse Models. *Elife* **2020**, *9*, 1–63, doi:10.7554/eLife.56551.
5. Shi, H.; Wang, H.; Zhang, C.; Lu, Y.; Yao, J.; Chen, Z.; Xing, G.; Wei, Q.; Cao, X. Mutations in OSBPL2 Cause Hearing Loss Associated with Primary Cilia Defects via Sonic Hedgehog Signaling. *JCI Insight* **2022**, *7*, doi:10.1172/jci.insight.149626.
6. Baird, R.A. Comparative Transduction Mechanisms of Hair Cells in the Bullfrog Utriculus. II. Sensitivity and Response Dynamics to Hair Bundle Displacement. *J Neurophysiol* **1994**, *71*, 685–705, doi:10.1152/jn.1994.71.2.685.
7. Spoon, C.; Grant, W. Biomechanics of Hair Cell Kinocilia: Experimental Measurement of Kinocilium Shaft Stiffness and Base Rotational Stiffness with Euler–Bernoulli and Timoshenko Beam Analysis. *Journal of Experimental Biology* **2011**, *214*, 862–870, doi:10.1242/jeb.051151.
8. Kindt, K.S.; Finch, G.; Nicolson, T. Kinocilia Mediate Mechanosensitivity in Developing Zebrafish Hair Cells. *Dev Cell* **2012**, *23*, 329–341, doi:10.1016/j.devcel.2012.05.022.
9. Stooke-Vaughan, G.A.; Huang, P.; Hammond, K.L.; Schier, A.F.; Whitfield, T.T. The Role of Hair Cells, Cilia and Ciliary Motility in Otolith Formation in the Zebrafish Otic Vesicle. *Development* **2012**, *139*, 1777–1787, doi:10.1242/dev.079947.
10. Sobkowicz, H.M.; Slapnick, S.M.; August, B.K. The Kinocilium of Auditory Hair Cells and Evidence for Its Morphogenetic Role during the Regeneration of Stereocilia and Cuticular Plates. *J Neurocytol* **1995**, *24*, 633–653, doi:10.1007/BF01179815.
11. Flock, A.; Duvall, A.J. The Ultrastructure of the Kinocilium of the Sensory Cells in the Inner Ear and Lateral Line Organs. *Journal of Cell Biology* **1965**, *25*, 1–8, doi:10.1083/jcb.25.1.1.
12. Kikuchi, T.; Takasaka, T.; Tonosaki, A.; Watanabe, H. Fine Structure of Guinea Pig Vestibular Kinocilium. *Acta Otolaryngol* **1989**, *108*, 26–30, doi:10.3109/00016488909107388.
13. Burton, P.R. Ultrastructural Studies of Microtubules and Microtubule Organizing Centers of the Vertebrate Olfactory Neuron. *Microsc Res Tech* **1992**, *23*, 142–156, doi:10.1002/jemt.1070230205.

14. Rüsch, A.; Thurm, U. Passive and Active Deflections of Ampullary Kinocilia Correlated with Changes in Transepithelial Voltage. *ORL* **1986**, *48*, 76–80, doi:10.1159/000275849.

15. Rüsch, A.; Thurm, U. Spontaneous and Electrically Induced Movements of Ampullary Kinocilia and Stereovilli. *Hear Res* **1990**, *48*, 247–263, doi:10.1016/0378-5955(90)90065-W.

16. Alstrom, C.H.; Hallgren, B.; Nilsson, L.; Asander, H. Retinal Degeneration Combined with Obesity, Diabetes Mellitus and Neurogenous Deafness: A Specific Syndrome (Not Hitherto Described) Distinct from the Laurence-Moon-Bardet-Biedl Syndrome: A Clinical, Endocrinological and Genetic Examination Based on a Large Pedigree. *Acta Psychiatr Neurol Scand Suppl* **1959**, *129*, 1–35.

17. Ross, A.J.; May-Simera, H.; Eichers, E.R.; Kai, M.; Hill, J.; Jagger, D.J.; Leitch, C.C.; Chapple, J.P.; Munro, P.M.; Fisher, S.; et al. Disruption of Bardet-Biedl Syndrome Ciliary Proteins Perturbs Planar Cell Polarity in Vertebrates. *Nature Genetics 2005 37:10* **2005**, *37*, 1135–1140, doi:10.1038/ng1644.

18. Jagger, D.; Collin, G.; Kelly, J.; Towers, E.; Nevill, G.; Longo-Guess, C.; Benson, J.; Halsey, K.; Dolan, D.; Marshall, J.; et al. Alström Syndrome Protein ALMS1 Localizes to Basal Bodies of Cochlear Hair Cells and Regulates Cilium-Dependent Planar Cell Polarity. *Hum Mol Genet* **2011**, *20*, 466–481, doi:10.1093/hmg/ddq493.

19. Modamio-Høybjør, S.; Mencía, Á.; Goodyear, R.; del Castillo, I.; Richardson, G.; Moreno, F.; Moreno-Pelayo, M.Á. A Mutation in CCDC50, a Gene Encoding an Effector of Epidermal Growth Factor-Mediated Cell Signaling, Causes Progressive Hearing Loss. *Am J Hum Genet* **2007**, *80*, 1076–1089, doi:10.1086/518311.

20. Cui, L.; Zheng, J.; Zhao, Q.; Chen, J.-R.; Liu, H.; Peng, G.; Wu, Y.; Chen, C.; He, Q.; Shi, H.; et al. Mutations of MAP1B Encoding a Microtubule-Associated Phosphoprotein Cause Sensorineural Hearing Loss. *JCI Insight* **2020**, *5*, doi:10.1172/jci.insight.136046.

21. Grati, M.; Chakchouk, I.; Ma, Q.; Bensaid, M.; Desmidt, A.; Turki, N.; Yan, D.; Baanannou, A.; Mittal, R.; Driss, N.; et al. A Missense Mutation in DCDC2 Causes Human Recessive Deafness DFNB66, Likely by Interfering with Sensory Hair Cell and Supporting Cell Cilia Length Regulation. *Hum Mol Genet* **2015**, *24*, 2482–2491, doi:10.1093/hmg/ddv009.

22. Bork, J.M.; Peters, L.M.; Riazuddin, S.; Ahmed, Z.M.; Li, X.C.; Griffith, A.J.; Wilcox, E.R.; Friedman, T.B.; Morell, R.J.; Griffith, A.J.; et al. Usher Syndrome 1D and Nonsyndromic Autosomal Recessive Deafness DFNB12 Are Caused by Allelic Mutations of the Novel Cadherin-like Gene CDH23. *Am J Hum Genet* **2001**, *68*, 26–37, doi:10.1086/316954.

23. Ahmed, Z.M. PCDH15 Is Expressed in the Neurosensory Epithelium of the Eye and Ear and Mutant Alleles Are Responsible for Both USH1F and DFNB23. *Hum Mol Genet* **2003**, *12*, 3215–3223, doi:10.1093/hmg/ddg358.

24. Goodman, L.; Zallocchi, M. Integrin A8 and Pcdh15 Act as a Complex to Regulate Cilia Biogenesis in Sensory Cells. *J Cell Sci* **2017**, *130*, 3698–3712, doi:10.1242/jcs.206201.

25. Pickett, S.B.; Raible, D.W. Water Waves to Sound Waves: Using Zebrafish to Explore Hair Cell Biology. *Journal of the Association for Research in Otolaryngology* **2019**, *20*, 1–19, doi:10.1007/s10162-018-00711-1.

26. Gunn, R.K.; Keenan, M.-E.; Brown, R.E. Analysis of Sensory, Motor and Cognitive Functions of the Coloboma (C3Sn.Cg-Cm/J) Mutant Mouse. *Genes Brain Behav* **2011**, *10*, 579–588, doi:10.1111/j.1601-183X.2011.00697.x.

27. Kiernan, A.E.; Ahituv, N.; Fuchs, H.; Balling, R.; Avraham, K.B.; Steel, K.P.; Hrabé de Angelis, M. The Notch Ligand Jagged1 Is Required for Inner Ear Sensory Development. *Proc Natl Acad Sci U S A* **2001**, *98*, 3873–3878, doi:10.1073/pnas.071496998.

28. Shen, J.; Scheffer, D.I.; Kwan, K.Y.; Corey, D.P. SHIELD: An Integrative Gene Expression Database for Inner Ear Research. *Database (Oxford)* **2015**, *2015*, bav071, doi:10.1093/database/bav071.

29. Westerfield, M. *The Zebrafish Book. A Guide for the Laboratory Use of Zebrafish (Danio Rerio).*; 4th ed.; University of Oregon: Eugene OR, 2000;

30. Ohta, S.; Ji, Y.R.; Martin, D.; Wu, D.K. Emx2 Regulates Hair Cell Rearrangement but Not Positional Identity within Neuromasts. *Elife* **2020**, *9*, 1–69, doi:10.7554/eLife.60432.

31. Erickson, T.; Pacentine, I. V; Venuto, A.; Clemens, R.; Nicolson, T. The Lhfpl5 Ohnologs Lhfpl5a and Lhfpl5b Are Required for Mechanotransduction in Distinct Populations of Sensory Hair Cells in Zebrafish. *Front Mol Neurosci* **2020**, *12*, 320, doi:10.3389/fnmol.2019.00320.

32. Erickson, T.; Nicolson, T. Identification of Sensory Hair-Cell Transcripts by Thiouracil-Tagging in Zebrafish. *BMC Genomics* **2015**, *16*, 842, doi:10.1186/s12864-015-2072-5.

33. Kwan, K.M.; Fujimoto, E.; Grabher, C.; Mangum, B.D.; Hardy, M.E.; Campbell, D.S.; Parant, J.M.; Yost, H.J.; Kanki, J.P.; Chien, C.-B. The Tol2kit: A Multisite Gateway-Based Construction Kit for Tol2 Transposon Transgenesis Constructs. *Developmental Dynamics* **2007**, *236*, 3088–3099, doi:10.1002/dvdy.21343.

34. Afgan, E.; Baker, D.; van den Beek, M.; Blankenberg, D.; Bouvier, D.; Čech, M.; Chilton, J.; Clements, D.; Coraor, N.; Eberhard, C.; et al. The Galaxy Platform for Accessible, Reproducible and Collaborative Biomedical Analyses: 2016 Update. *Nucleic Acids Res* **2016**, *44*, W3–W10, doi:10.1093/nar/gkw343.

35. Thomas, P.D.; Ebert, D.; Muruganujan, A.; Mushayahama, T.; Albou, L.-P.; Mi, H. PANTHER: Making Genome-Scale Phylogenetics Accessible to All. *Protein Sci* **2022**, *31*, 8–22, doi:10.1002/pro.4218.

36. Mi, H.; Muruganujan, A.; Huang, X.; Ebert, D.; Mills, C.; Guo, X.; Thomas, P.D. Protocol Update for Large-Scale Genome and Gene Function Analysis with the PANTHER Classification System (v.14.0). *Nature Protocols 2019 14:3* **2019**, *14*, 703–721, doi:10.1038/s41596-019-0128-8.

37. van Camp, G.; Smith, R.J.H. Hereditary Hearing Loss Homepage Available online: https://hereditaryhearingloss.org (accessed on 29 December 2022).

38. Cunningham, F.; Allen, J.E.; Allen, J.; Alvarez-Jarreta, J.; Amode, M.R.; Armean, I.M.; Austine-Orimoloye, O.; Azov, A.G.; Barnes, I.; Bennett, R.; et al. Ensembl 2022. *Nucleic Acids Res* **2022**, *50*, D988–D995, doi:10.1093/NAR/GKAB1049.

39. Daniel, J.G.; Panizzi, J.R. Spatiotemporal Expression Profile of Embryonic and Adult Ankyrin Repeat and EF-Hand Domain Containing Protein 1-Encoding Genes Ankef1a and Ankef1b in Zebrafish. *Gene Expression Patterns* **2019**, *34*, 119069, doi:10.1016/j.gep.2019.119069.

40. Schindelin, J.; Arganda-Carreras, I.; Frise, E.; Kaynig, V.; Longair, M.; Pietzsch, T.; Preibisch, S.; Rueden, C.; Saalfeld, S.; Schmid, B.; et al. Fiji: An Open-Source Platform for Biological-Image Analysis. *Nat Methods* **2012**, *9*, 676–682, doi:10.1038/nmeth.2019.

41. Schneider, C.A.; Rasband, W.S.; Eliceiri, K.W. NIH Image to ImageJ: 25 Years of Image Analysis. *Nat Methods* **2012**, *9*, 671–675, doi:10.1038/nmeth.2089.

42. Arshadi, C.; Günther, U.; Eddison, M.; Harrington, K.I.S.; Ferreira, T.A. SNT: A Unifying Toolbox for Quantification of Neuronal Anatomy. *Nature Methods 2021 18:4* **2021**, *18*, 374–377, doi:10.1038/s41592-021-01105-7.

43. RStudio Team RStudio: Integrated Development Environment for R 2022.

44. R Core Team R: A Language and Environment for Statistical Computing 2022.

45. Wickham, H. Ggplot2. *Wiley Interdiscip Rev Comput Stat* **2011**, *3*, 180–185, doi:10.1002/wics.147.

46. Miller, M.R.; Robinson, K.J.; Cleary, M.D.; Doe, C.Q. TU-Tagging: Cell Type-Specific RNA Isolation from Intact Complex Tissues. *Nat Methods* **2009**, *6*, 439–441, doi:10.1038/nmeth.1329.

47. Scott, E.K.; Mason, L.; Arrenberg, A.B.; Ziv, L.; Gosse, N.J.; Xiao, T.; Chi, N.C.; Asakawa, K.; Kawakami, K.; Baier, H. Targeting Neural Circuitry in Zebrafish Using GAL4 Enhancer Trapping. *Nature Methods 2007 4:4* **2007**, *4*, 323–326, doi:10.1038/nmeth1033.

48. Chung, H.A.; Yamamoto, T.S.; Ueno, N. ANR5, an FGF Target Gene Product, Regulates Gastrulation in Xenopus. *Current Biology* **2007**, *17*, 932–939, doi:10.1016/j.cub.2007.04.034.

49. di Domenico, F. The Role of Ankef1 in Male Fertility, Icahn School of Medicine at Mount Sinai: New York, 2021.

50. Jan, T.A.; Eltawil, Y.; Ling, A.H.; Chen, L.; Ellwanger, D.C.; Heller, S.; Cheng, A.G. Spatiotemporal Dynamics of Inner Ear Sensory and Non-Sensory Cells Revealed by Single-Cell Transcriptomics. *Cell Rep* **2021**, *36*, 109358, doi:10.1016/j.celrep.2021.109358.

51. Hoh, R.A.; Stowe, T.R.; Turk, E.; Stearns, T. Transcriptional Program of Ciliated Epithelial Cells Reveals New Cilium and Centrosome Components and Links to Human Disease. *PLoS One* **2012**, *7*, e52166, doi:10.1371/journal.pone.0052166.

52. Baker, M.A.; Hetherington, L.; Reeves, G.M.; Aitken, R.J. The Mouse Sperm Proteome Characterizedvia IPG Strip Prefractionation and LC-MS/MS Identification. *Proteomics* **2008**, *8*, 1720–1730, doi:10.1002/pmic.200701020.

53. Baker, M.A.; Hetherington, L.; Reeves, G.; Müller, J.; Aitken, R.J. The Rat Sperm Proteome Characterized ***via*** IPG Strip Prefractionation and LC-MS/MS Identification. *Proteomics* **2008**, *8*, 2312–2321, doi:10.1002/pmic.200700876.

54. Blackburn, K.; Bustamante-Marin, X.; Yin, W.; Goshe, M.B.; Ostrowski, L.E. Quantitative Proteomic Analysis of Human Airway Cilia Identifies Previously Uncharacterized Proteins of High Abundance. *J Proteome Res* **2017**, *16*, 1579–1592, doi:10.1021/acs.jproteome.6b00972.

55. Elkon, R.; Milon, B.; Morrison, L.; Shah, M.; Vijayakumar, S.; Racherla, M.; Leitch, C.C.; Silipino, L.; Hadi, S.; Weiss-Gayet, M.; et al. RFX Transcription Factors Are Essential for Hearing in Mice. *Nat Commun* **2015**, *6*, 8549, doi:10.1038/ncomms9549.

56. Lush, M.E.; Diaz, D.C.; Koenecke, N.; Baek, S.; Boldt, H.; St Peter, M.K.; Gaitan-Escudero, T.; Romero-Carvajal, A.; Busch-Nentwich, E.M.; Perera, A.G.; et al. ScRNA-Seq Reveals Distinct Stem Cell Populations That Drive Hair Cell Regeneration after Loss of Fgf and Notch Signaling. *Elife* **2019**, *8*, doi:10.7554/eLife.44431.

57. Barta, C.L.; Liu, H.; Chen, L.; Giffen, K.P.; Li, Y.; Kramer, K.L.; Beisel, K.W.; He, D.Z. RNA-Seq Transcriptomic Analysis of Adult Zebrafish Inner Ear Hair Cells. *Sci Data* **2018**, *5*, 180005, doi:10.1038/sdata.2018.5.

58. Hess, E.J.; Collins, K.A.; Copeland, N.G.; Jenkins, N.A.; Wilson, M.C. Deletion Map of the Coloboma (Cm) Locus on Mouse Chromosome 2. *Genomics* **1994**, *21*, 257–261, doi:10.1006/geno.1994.1254.

59. Blake, J.A.; Baldarelli, R.; Kadin, J.A.; Richardson, J.E.; Smith, C.L.; Bult, C.J.; Anagnostopoulos, A. v; Beal, J.S.; Bello, S.M.; Blodgett, O.; et al. Mouse Genome Database (MGD): Knowledgebase for Mouse–Human Comparative Biology. *Nucleic Acids Res* **2021**, *49*, D981–D987, doi:10.1093/nar/gkaa1083.

60. Hess, E.; Jinnah, H.; Kozak, C.; Wilson, M. Spontaneous Locomotor Hyperactivity in a Mouse Mutant with a Deletion Including the Snap Gene on Chromosome 2. *The Journal of Neuroscience* **1992**, *12*, 2865–2874, doi:10.1523/JNEUROSCI.12-07-02865.1992.

61. Egydio de Carvalho, C.; Tanaka, H.; Iguchi, N.; Ventelä, S.; Nojima, H.; Nishimune, Y. Molecular Cloning and Characterization of a Complementary DNA Encoding Sperm Tail Protein SHIPPO 11. *Biol Reprod* **2002**, *66*, 785–795, doi:10.1095/biolreprod66.3.785.

62. Dorus, S.; Busby, S.A.; Gerike, U.; Shabanowitz, J.; Hunt, D.F.; Karr, T.L. Genomic and Functional Evolution of the Drosophila Melanogaster Sperm Proteome. *Nat Genet* **2006**, *38*, 1440–1445, doi:10.1038/ng1915.

63. Konno, A.; Padma, P.; Ushimaru, Y.; Inaba, K. Multidimensional Analysis of Uncharacterized Sperm Proteins in *Ciona Intestinalis* : EST-Based Analysis and

Functional Immunoscreening of Testis-Expressed Genes. *Zoolog Sci* **2010**, *27*, 204–215, doi:10.2108/zsj.27.204.

64. Konno, A.; Shiba, K.; Cai, C.; Inaba, K. Branchial Cilia and Sperm Flagella Recruit Distinct Axonemal Components. *PLoS One* **2015**, *10*, e0126005, doi:10.1371/journal.pone.0126005.

65. White-Cooper, H. Studying How Flies Make Sperm—Investigating Gene Function in Drosophila Testes. *Mol Cell Endocrinol* **2009**, *306*, 66–74, doi:10.1016/j.mce.2008.11.026.

66. Bastin, B.R. Evolution of Tektin and ODF3 Family Genes and the Role of Gene Duplication in the Specialization of Motile Ciliary Structures in the Polychaete Platynereis Dumerilii, Iowa State University, 2018.

67. Lauwaet, T.; Smith, A.J.; Reiner, D.S.; Romijn, E.P.; Wong, C.C.L.; Davids, B.J.; Shah, S.A.; Yates, J.R.; Gillin, F.D. Mining the Giardia Genome and Proteome for Conserved and Unique Basal Body Proteins. *Int J Parasitol* **2011**, *41*, 1079–1092, doi:10.1016/j.ijpara.2011.06.001.

68. Fong, K.; Leung, J.W.; Li, Y.; Wang, W.; Feng, L.; Ma, W.; Liu, D.; Songyang, Z.; Chen, J. MTR120/KIAA1383, a Novel Microtubule-Associated Protein, Promotes Microtubule Stability and Ensures Cytokinesis. *J Cell Sci* **2013**, *126*, 825–837, doi:10.1242/jcs.116137.

69. Kubo, S.; Black, C.S.; Joachimiak, E.; Yang, S.K.; Legal, T.; Peri, K.; Abdelzaher, A.; Khalifa, Z.; Ghanaeian, A.; Mccafferty, C.L.; et al. Native Doublet Microtubules from Tetrahymena Thermophila Reveal the Importance of Outer Junction Proteins. *Nature Communications 2023 14:1* **2023**, *14*, 1–16, doi:10.1038/s41467-023-37868-0.

70. Bowl, M.R.; Simon, M.M.; Ingham, N.J.; Greenaway, S.; Santos, L.; Cater, H.; Taylor, S.; Mason, J.; Kurbatova, N.; Pearson, S.; et al. A Large Scale Hearing Loss Screen Reveals an Extensive Unexplored Genetic Landscape for Auditory Dysfunction. *Nat Commun* **2017**, *8*, 886, doi:10.1038/s41467-017-00595-4.

71. Ain, Q.; Nazli, S.; Riazuddin, S.; Jaleel, A.; Riazuddin, S.A.; Zafar, A.U.; Khan, S.N.; Husnain, T.; Griffith, A.J.; Ahmed, Z.M.; et al. The Autosomal Recessive Nonsyndromic Deafness Locus DFNB72 Is Located on Chromosome 19p13.3. *Hum Genet* **2007**, *122*, 445–450, doi:10.1007/s00439-007-0418-z.

72. Bönsch, D.; Schmidt, C.M.; Scheer, P.; Bohlender, J.; Neumann, C.; am Zehnhoff-Dinnesen, A.; Deufel, T. Ein Neuer Genort Für Eine Autosomal Dominante, Nichtsyndromale Hörstörung (DFNA57) Kartiert Auf Chromosom 19p13.2 Und Überlappt Mit DFNB15. *HNO* **2008**, *56*, 177–182, doi:10.1007/s00106-007-1633-6.

73. Mangino, M.; Flex, E.; Capon, F.; Sangiuolo, F.; Carraro, E.; Gualandi, F.; Mazzoli, M.; Martini, A.; Novelli, G.; Dallapiccola, B. Mapping of a New Autosomal Dominant Nonsyndromic Hearing Loss Locus (DFNA30) to Chromosome 15q25-26. *European Journal of Human Genetics* **2001**, *9*, 667–671, doi:10.1038/sj.ejhg.5200707.

74. Rehman, A.U.; Gul, K.; Morell, R.J.; Lee, K.; Ahmed, Z.M.; Riazuddin, S.; Ali, R.A.; Shahzad, M.; Jaleel, A.; Andrade, P.B.; et al. Mutations of GIPC3 Cause Nonsyndromic Hearing Loss DFNB72 but Not DFNB81 That Also Maps to Chromosome 19p. *Hum Genet* **2011**, *130*, 759–765, doi:10.1007/s00439-011-1018-5.

75. Charizopoulou, N.; Lelli, A.; Schraders, M.; Ray, K.; Hildebrand, M.S.; Ramesh, A.; Srisailapathy, C.R.S.; Oostrik, J.; Admiraal, R.J.C.; Neely, H.R.; et al. Gipc3 Mutations Associated with Audiogenic Seizures and Sensorineural Hearing Loss in Mouse and Human. *Nat Commun* **2011**, *2*, 201, doi:10.1038/ncomms1200.

76. Santos-Cortez, R.L.P.; Faridi, R.; Rehman, A.U.; Lee, K.; Ansar, M.; Wang, X.; Morell, R.J.; Isaacson, R.; Belyantseva, I.A.; Dai, H.; et al. Autosomal-Recessive Hearing Impairment Due to Rare Missense Variants within S1PR2. *Am J Hum Genet* **2016**, *98*, 331–338, doi:10.1016/j.ajhg.2015.12.004.

77. Jenkinson, E.M.; Rehman, A.U.; Walsh, T.; Clayton-Smith, J.; Lee, K.; Morell, R.J.; Drummond, M.C.; Khan, S.N.; Naeem, M.A.; Rauf, B.; et al. Perrault Syndrome Is Caused by Recessive Mutations in CLPP, Encoding a Mitochondrial ATP-Dependent Chambered Protease. *Am J Hum Genet* **2013**, *92*, 605–613, doi:10.1016/j.ajhg.2013.02.013.

78. Cuveillier, C.; Boulan, B.; Ravanello, C.; Denarier, E.; Deloulme, J.-C.; Gory-Fauré, S.; Delphin, C.; Bosc, C.; Arnal, I.; Andrieux, A. Beyond Neuronal Microtubule Stabilization: MAP6 and CRMPS, Two Converging Stories. *Front Mol Neurosci* **2021**, *14*, 82, doi:10.3389/fnmol.2021.665693.

79. Dacheux, D.; Landrein, N.; Thonnus, M.; Gilbert, G.; Sahin, A.; Wodrich, H.; Robinson, D.R.; Bonhivers, M. A MAP6-Related Protein Is Present in Protozoa and Is Involved in Flagellum Motility. *PLoS One* **2012**, *7*, e31344, doi:10.1371/journal.pone.0031344.

80. Dacheux, D.; Roger, B.; Bosc, C.; Landrein, N.; Roche, E.; Chansel, L.; Trian, T.; Andrieux, A.; Papaxanthos-Roche, A.; Marthan, R.; et al. Human FAM154A (SAXO1) Is a Microtubule-Stabilizing Protein Specific to Cilia and Related Structures. *J Cell Sci* **2015**, *128*, 1294–1307, doi:10.1242/jcs.155143.

81. Onyeneho, I.A. Microtubule Stability Mediated by New Mammalian STOP Family Members, Stanford University, 2014.

82. Kim, K.; Gibboney, S.; Razy-Krajka, F.; Lowe, E.K.; Wang, W.; Stolfi, A. Regulation of Neurogenesis by FGF Signaling and Neurogenin in the Invertebrate Chordate Ciona. *Front Cell Dev Biol* **2020**, *8*, 477, doi:10.3389/fcell.2020.00477.

83. Leung, M.R.; Roelofs, M.C.; Chiozzi, R.Z.; Hevler, J.F.; Heck, A.J.R.; Zeev-Ben-Mordehai, T. Unraveling the Intricate Microtubule Inner Protein Networks That Reinforce Mammalian Sperm Flagella. *bioRxiv* **2022**, 2022.09.29.510157, doi:10.1101/2022.09.29.510157.

84. Gui, M.; Wang, X.; Dutcher, S.K.; Brown, A.; Zhang, R. Ciliary Central Apparatus Structure Reveals Mechanisms of Microtubule Patterning. *Nat Struct Mol Biol* **2022**, *29*, 483–492, doi:10.1038/s41594-022-00770-2.

85. Gui, M.; Croft, J.T.; Zabeo, D.; Acharya, V.; Kollman, J.M.; Burgoyne, T.; Höög, J.L.; Brown, A. SPACA9 Is a Lumenal Protein of Human Ciliary Singlet and Doublet Microtubules. *Proc Natl Acad Sci U S A* **2022**, *119*, e2207605119, doi:10.1073/pnas.2207605119.

86. Ichikawa, M.; Bui, K.H. Microtubule Inner Proteins: A Meshwork of Luminal Proteins Stabilizing the Doublet Microtubule. *BioEssays* **2018**, *40*, 1700209, doi:10.1002/bies.201700209.

87. Cuveillier, C.; Delaroche, J.; Seggio, M.; Gory-Fauré, S.; Bosc, C.; Denarier, E.; Bacia, M.; Schoehn, G.; Mohrbach, H.; Kulić, I.; et al. MAP6 Is an Intraluminal Protein That Induces Neuronal Microtubules to Coil. *Sci Adv* **2020**, *6*, doi:10.1126/sciadv.aaz4344.

88. Wilkerson, B.A.; Zebroski, H.L.; Finkbeiner, C.R.; Chitsazan, A.D.; Beach, K.E.; Sen, N.; Zhang, R.C.; Bermingham-McDonogh, O. Novel Cell Types and Developmental Lineages Revealed by Single-Cell RNA-Seq Analysis of the Mouse Crista Ampullaris. *Elife* **2021**, *10*, doi:10.7554/eLife.60108.

89. Azaiez, H.; Decker, A.R.; Booth, K.T.; Simpson, A.C.; Shearer, A.E.; Huygen, P.L.M.; Bu, F.; Hildebrand, M.S.; Ranum, P.T.; Shibata, S.B.; et al. HOMER2, a Stereociliary Scaffolding Protein, Is Essential for Normal Hearing in Humans and Mice. *PLoS Genet* **2015**, *11*, e1005137, doi:10.1371/journal.pgen.1005137.

90. Lu, X.; Wang, Q.; Gu, H.; Zhang, X.; Qi, Y.; Liu, Y. Whole Exome Sequencing Identified a Second Pathogenic Variant in HOMER2 for Autosomal Dominant Non-Syndromic Deafness. *Clin Genet* **2018**, *94*, 419–428, doi:10.1111/cge.13422.

91. Ahmad, J.; Khan, S.N.; Khan, S.Y.; Ramzan, K.; Riazuddin, S.; Ahmed, Z.M.; Wilcox, E.R.; Friedman, T.B.; Riazuddin, S. DFNB48, a New Nonsyndromic Recessive Deafness Locus, Maps to Chromosome 15q23-Q25.1. *Hum Genet* **2005**, *116*, 407–412, doi:10.1007/s00439-004-1247-y.

92. Riazuddin, S.; Belyantseva, I.A.; Giese, A.P.J.; Lee, K.; Indzhykulian, A.A.; Nandamuri, S.P.; Yousaf, R.; Sinha, G.P.; Lee, S.; Terrell, D.; et al. Alterations of the CIB2 Calcium- and Integrin-Binding Protein Cause Usher Syndrome Type 1J and Nonsyndromic Deafness DFNB48. *Nat Genet* **2012**, *44*, 1265–1271, doi:10.1038/ng.2426.

93. Tomek, M.S.; Brown, M.R.; Mani, S.R.; Ramesh, A.; Srisailapathy, C.R.; Coucke, P.; Zbar, R.I.; Bell, A.M.; McGuirt, W.T.; Fukushima, K.; et al. Localization of a Gene for Otosclerosis to Chromosome 15q25-Q26. *Hum Mol Genet* **1998**, *7*, 285–290, doi:10.1093/hmg/7.2.285.

94. Wang, S.; Hazelrigg, T. Implications for Bcd MRNA Localization from Spatial Distribution of Exu Protein in Drosophila Oogenesis. *Nature* **1994**, *369*, 400–403, doi:10.1038/369400a0.

95. Gerdes, H.-H.; Kaether, C. Green Fluorescent Protein: Applications in Cell Biology. *FEBS Lett* **1996**, *389*, 44–47, doi:10.1016/0014-5793(96)00586-8.

96. Sheets, L.; He, X.J.; Olt, J.; Schreck, M.; Petralia, R.S.; Wang, Y.-X.; Zhang, Q.; Beirl, A.; Nicolson, T.; Marcotti, W.; et al. Enlargement of Ribbons in Zebrafish Hair

Cells Increases Calcium Currents But Disrupts Afferent Spontaneous Activity and Timing of Stimulus Onset. *The Journal of Neuroscience* **2017**, *37*, 6299–6313, doi:10.1523/JNEUROSCI.2878-16.2017.

97. Maeda, R.; Pacentine, I. v; Erickson, T.; Nicolson, T. Functional Analysis of the Transmembrane and Cytoplasmic Domains of Pcdh15a in Zebrafish Hair Cells. *J Neurosci* **2017**, *37*, 3231–3245, doi:10.1523/JNEUROSCI.2216-16.2017.

98. Erickson, T.; Morgan, C.P.; Olt, J.; Hardy, K.; Busch-Nentwich, E.; Maeda, R.; Clemens, R.; Krey, J.F.; Nechiporuk, A.; Barr-Gillespie, P.G.; et al. Integration of Tmc1/2 into the Mechanotransduction Complex in Zebrafish Hair Cells Is Regulated by Transmembrane O-Methyltransferase (Tomt). *Elife* **2017**, *6*, doi:10.7554/eLife.28474.

99. Pacentine, I. v.; Nicolson, T. Subunits of the Mechano-Electrical Transduction Channel, Tmc1/2b, Require Tmie to Localize in Zebrafish Sensory Hair Cells. *PLoS Genet* **2019**, *15*, e1007635, doi:10.1371/journal.pgen.1007635.

100. Gopal, S.R.; Chen, D.H.-C.; Chou, S.-W.; Zang, J.; Neuhauss, S.C.F.; Stepanyan, R.; McDermott, B.M.; Alagramam, K.N. Zebrafish Models for the Mechanosensory Hair Cell Dysfunction in Usher Syndrome 3 Reveal That Clarin-1 Is an Essential Hair Bundle Protein. *Journal of Neuroscience* **2015**, *35*, 10188–10201, doi:10.1523/JNEUROSCI.1096-15.2015.

101. Smith, E.T.; Pacentine, I.; Shipman, A.; Hill, M.; Nicolson, T. Disruption of *Tmc1/2a/2b* Genes in Zebrafish Reveals Subunit Requirements in Subtypes of Inner Ear Hair Cells. *The Journal of Neuroscience* **2020**, *40*, 4457–4468, doi:10.1523/JNEUROSCI.0163-20.2020.

102. Chen, Z.; Chou, S.-W.; McDermott, B.M. Ribeye Protein Is Intrinsically Dynamic but Is Stabilized in the Context of the Ribbon Synapse. *J Physiol* **2018**, *596*, 409–421, doi:10.1113/JP271215.

103. Hwang, P.; Chou, S.-W.; Chen, Z.; McDermott, B.M. The Stereociliary Paracrystal Is a Dynamic Cytoskeletal Scaffold In Vivo. *Cell Rep* **2015**, *13*, 1287–1294, doi:10.1016/j.celrep.2015.10.003.

104. Sheets, L.; Hagen, M.W.; Nicolson, T. Characterization of Ribeye Subunits in Zebrafish Hair Cells Reveals That Exogenous Ribeye B-Domain and CtBP1 Localize to the Basal Ends of Synaptic Ribbons. *PLoS One* **2014**, *9*, e107256, doi:10.1371/journal.pone.0107256.

105. Choksi, S.P.; Babu, D.; Lau, D.; Yu, X.; Roy, S. Systematic Discovery of Novel Ciliary Genes through Functional Genomics in the Zebrafish. *Development* **2014**, *141*, 3410–3419, doi:10.1242/dev.108209.

106. Walentek, P.; Quigley, I.K.; Sun, D.I.; Sajjan, U.K.; Kintner, C.; Harland, R.M. Ciliary Transcription Factors and MiRNAs Precisely Regulate Cp110 Levels Required for Ciliary Adhesions and Ciliogenesis. *Elife* **2016**, *5*, doi:10.7554/eLife.17557.

107. Stauber, M.; Weidemann, M.; Dittrich-Breiholz, O.; Lobschat, K.; Alten, L.; Mai, M.; Beckers, A.; Kracht, M.; Gossler, A. Identification of FOXJ1 Effectors during

Ciliogenesis in the Foetal Respiratory Epithelium and Embryonic Left-Right Organiser of the Mouse. *Dev Biol* **2017**, *423*, 170–188, doi:10.1016/j.ydbio.2016.11.019.

108. Alsolami, M.; Kuhns, S.; Alsulami, M.; Blacque, O.E. ERICH3 in Primary Cilia Regulates Cilium Formation and the Localisations of Ciliary Transport and Sonic Hedgehog Signaling Proteins. *Scientific Reports 2019 9:1* **2019**, *9*, 1–13, doi:10.1038/s41598-019-52830-1.

109. Imtiaz, A.; Belyantseva, I.A.; Beirl, A.J.; Fenollar-Ferrer, C.; Bashir, R.; Bukhari, I.; Bouzid, A.; Shaukat, U.; Azaiez, H.; Booth, K.T.; et al. CDC14A Phosphatase Is Essential for Hearing and Male Fertility in Mouse and Human. *Hum Mol Genet* **2018**, *27*, 780–798, doi:10.1093/hmg/ddx440.

110. Schwenk, B.M.; Lang, C.M.; Hogl, S.; Tahirovic, S.; Orozco, D.; Rentzsch, K.; Lichtenthaler, S.F.; Hoogenraad, C.C.; Capell, A.; Haass, C.; et al. The FTLD Risk Factor TMEM106B and MAP6 Control Dendritic Trafficking of Lysosomes. *EMBO J* **2013**, *33*, n/a-n/a, doi:10.1002/embj.201385857.

111. Gory-Fauré, S.; Windscheid, V.; Brocard, J.; Montessuit, S.; Tsutsumi, R.; Denarier, E.; Fukata, Y.; Bosc, C.; Delaroche, J.; Collomb, N.; et al. Non-Microtubular Localizations of Microtubule-Associated Protein 6 (MAP6). *PLoS One* **2014**, *9*, e114905, doi:10.1371/journal.pone.0114905.

112. Tortosa, E.; Adolfs, Y.; Fukata, M.; Pasterkamp, R.J.; Kapitein, L.C.; Hoogenraad, C.C. Dynamic Palmitoylation Targets MAP6 to the Axon to Promote Microtubule Stabilization during Neuronal Polarization. *Neuron* **2017**, *94*, 809-825.e7, doi:10.1016/j.neuron.2017.04.042.

113. Lu, Q.; Insinna, C.; Ott, C.; Stauffer, J.; Pintado, P.A.; Rahajeng, J.; Baxa, U.; Walia, V.; Cuenca, A.; Hwang, Y.S.; et al. Early Steps in Primary Cilium Assembly Require EHD1/EHD3-Dependent Ciliary Vesicle Formation. *Nature Cell Biology 2014 17:3* **2015**, *17*, 228–240, doi:10.1038/ncb3109.

114. Lee, J.; Chung, Y.D. Ciliary Subcompartments: How Are They Established and What Are Their Functions? *BMB Rep* **2015**, *48*, 380–387, doi:10.5483/BMBRep.2015.48.7.084.

115. Soares, H.; Carmona, B.; Nolasco, S.; Melo, L.V.; Gonçalves, J. Cilia Distal Domain: Diversity in Evolutionarily Conserved Structures. *Cells 2019, Vol. 8, Page 160* **2019**, *8*, 160, doi:10.3390/CELLS8020160.

116. Gui, M.; Farley, H.; Anujan, P.; Anderson, J.R.; Maxwell, D.W.; Whitchurch, J.B.; Botsch, J.J.; Qiu, T.; Meleppattu, S.; Singh, S.K.; et al. De Novo Identification of Mammalian Ciliary Motility Proteins Using Cryo-EM. *Cell* **2021**, *184*, 5791-5806.e19, doi:10.1016/j.cell.2021.10.007.

117. Lagziel, A.; Ahmed, Z.M.; Schultz, J.M.; Morell, R.J.; Belyantseva, I.A.; Friedman, T.B. Spatiotemporal Pattern and Isoforms of Cadherin 23 in Wild Type and Waltzer Mice during Inner Ear Hair Cell Development. *Dev Biol* **2005**, *280*, 295–306, doi:10.1016/j.ydbio.2005.01.015.

118. Nicolson, T.; Rüsch, A.; Friedrich, R.W.; Granato, M.; Ruppersberg, J.P.; Nüsslein-Volhard, C. Genetic Analysis of Vertebrate Sensory Hair Cell Mechanosensation: The Zebrafish Circler Mutants. *Neuron* **1998**, *20*, 271–283, doi:10.1016/S0896-6273(00)80455-9.

119. Lanford, P.J.; Lan, Y.; Jiang, R.; Lindsell, C.; Weinmaster, G.; Gridley, T.; Kelley, M.W. Notch Signalling Pathway Mediates Hair Cell Development in Mammalian Cochlea. *Nature Genetics 1999 21:3* **1999**, *21*, 289–292, doi:10.1038/6804.

120. Zine, A.; van de Water, T.R.; de Ribaupierre, F. Notch Signaling Regulates the Pattern of Auditory Hair Cell Differentiation in Mammals. *Development* **2000**, *127*, 3373–3383, doi:10.1242/dev.127.15.3373.

121. Bowl, M.R.; Brown, S.D.M. Genetic Landscape of Auditory Dysfunction. *Hum Mol Genet* **2018**, *27*, R130–R135, doi:10.1093/hmg/ddy158.

122. Groza, T.; Gomez, F.L.; Mashhadi, H.H.; Muñoz-Fuentes, V.; Gunes, O.; Wilson, R.; Cacheiro, P.; Frost, A.; Keskivali-Bond, P.; Vardal, B.; et al. The International Mouse Phenotyping Consortium: Comprehensive Knockout Phenotyping Underpinning the Study of Human Disease. *Nucleic Acids Res* **2022**, doi:10.1093/nar/gkac972.

123. Kolla, L.; Kelly, M.C.; Mann, Z.F.; Anaya-Rocha, A.; Ellis, K.; Lemons, A.; Palermo, A.T.; So, K.S.; Mays, J.C.; Orvis, J.; et al. Characterization of the Development of the Mouse Cochlear Epithelium at the Single Cell Level. *Nature Communications 2020 11:1* **2020**, *11*, 1–16, doi:10.1038/s41467-020-16113-y.

124. Kubota, M.; Scheibinger, M.; Jan, T.A.; Heller, S. Greater Epithelial Ridge Cells Are the Principal Organoid-Forming Progenitors of the Mouse Cochlea. *Cell Rep* **2021**, *34*, 108646, doi:10.1016/j.celrep.2020.108646.

125. Steiner, A.B.; Kim, T.; Cabot, V.; Hudspeth, A.J. Dynamic Gene Expression by Putative Hair-Cell Progenitors during Regeneration in the Zebrafish Lateral Line. *Proc Natl Acad Sci U S A* **2014**, *111*, E1393-401, doi:10.1073/pnas.1318692111.

126. Liu, Y.; Pathak, N.; Kramer-Zucker, A.; Drummond, I.A. Notch Signaling Controls the Differentiation of Transporting Epithelia and Multiciliated Cells in the Zebrafish Pronephros. *Development* **2007**, *134*, 1111–1122, doi:10.1242/dev.02806.

127. Hsu, C.-C.; Hou, M.-F.; Hong, J.-R.; Wu, J.-L.; Her, G.M. Inducible Male Infertility by Targeted Cell Ablation in Zebrafish Testis. *Mar Biotechnol (NY)* **2010**, *12*, 466–478, doi:10.1007/s10126-009-9248-4.

7. Supplemental Figures

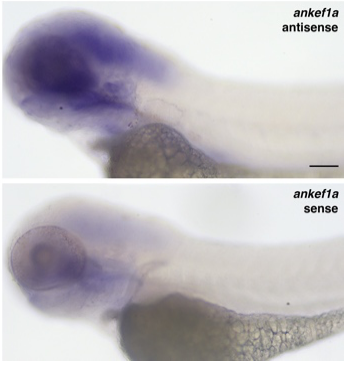

Figure S1. Wholemount mRNA in situ hybridization (ISH) for *ankef1a* on 3-day post-fertilization zebrafish larvae using antisense (top) and sense (bottom) DIG-labeled probes targeted to nucleotides 1912-2687 of ENSDART00000153006.2. Primers used to generate the *ankef1a* ISH probe templates are detailed in Table S1. Scale bar = 100 µm.

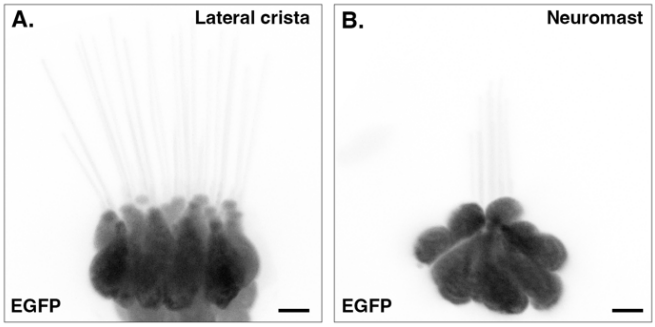

Figure S2. EGFP localization in hair cells of a lateral crista (**A**) and lateral line neuromast (**B**) in a *Tg(myo6b:EGFP)vo68* transgenic zebrafish at 5 days post-fertilization. Scale bars = 5 µm.

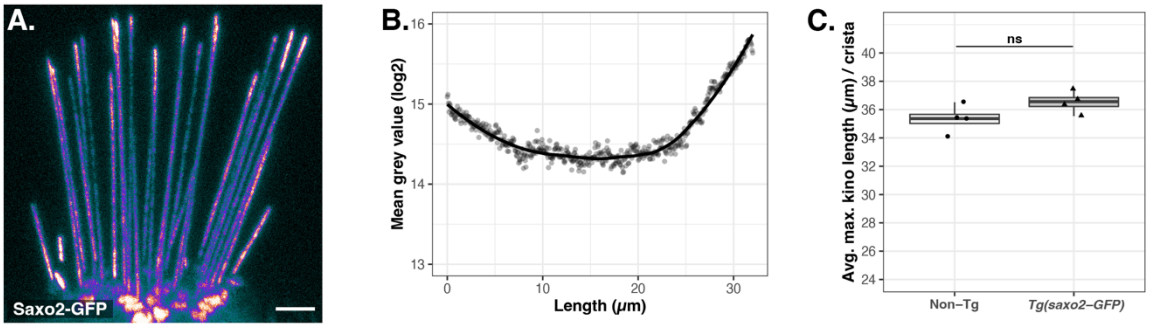

Figure S3. Saxo2-GFP kinocilial distribution and effect on kinocilia height. **A.** Pixel intensity-encoded image of Saxo2-GFP in the kinocilia of lateral cristae hair cells at 5 days post-fertilization (dpf). Brighter colours indicate higher fluorescence intensity. **B.** Scatter plot of averaged mean grey values (log2) for fluorescence intensity from kinocilia in the lateral cristae of Saxo2-GFP transgenics (n = 16 kinocilia from 4 individuals at 5 dpf). Position 0 µm is from the proximal region near the base of kinocilia and position 32 µm is the distal-most tip. **C.** Boxplots of maximum kinocilia length in the lateral crista of *saxo2-GFP* transgenics and their non-transgenic siblings at 5 dpf. Data points are the average length of the five tallest kinocilia from an individual larva. Two-tailed Welch's t-test statistics: non-Tg, n = 4 larvae, mean = 35.3 µm; *Tg(saxo2-GFP)*, n = 4, mean = 36.5 µm; t = -1.8712, df = 5.5674, p = 0.1143. Scale bar is 5 µm in A.

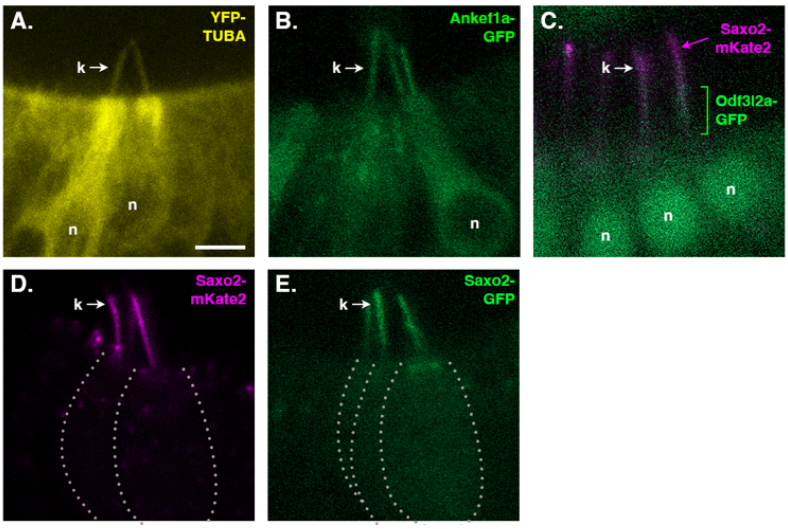

Figure S4. Transgenic protein localization in hair cells of the anterior macula: **A.** YFP-TUBA; **B.** Ankef1a-GFP; **C.** Odf3l2a-GFP with Saxo2-mKate2; **D.** Saxo2-mKate2; **E.** Saxo2-GFP. All images are from 1-day post-fertilization (dpf) larvae, except panel C which is at 5 dpf due to low fluorescence intensity for Odf3l2a-GFP at 1 dpf. Approximate cell outlines are indicated by dashed lines in panels D and E. k = kinocilium, n = nucleus. Scale bar = 5 µm, applies to all images.

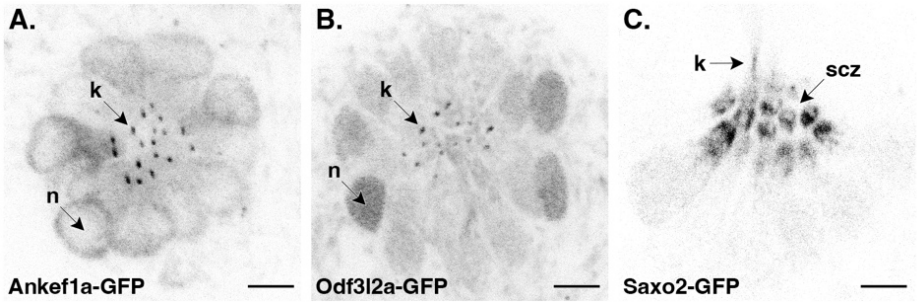

Figure S5. Ankef1a-GFP (**A**), Odf3l2a-GFP (**B**), and Saxo2-GFP (**C**) localization patterns in the soma of neuromast hair cells (top-down views). k = kinocilium, n = nucleus, scz = subcuticular zone. Scale bars = 5 µm.

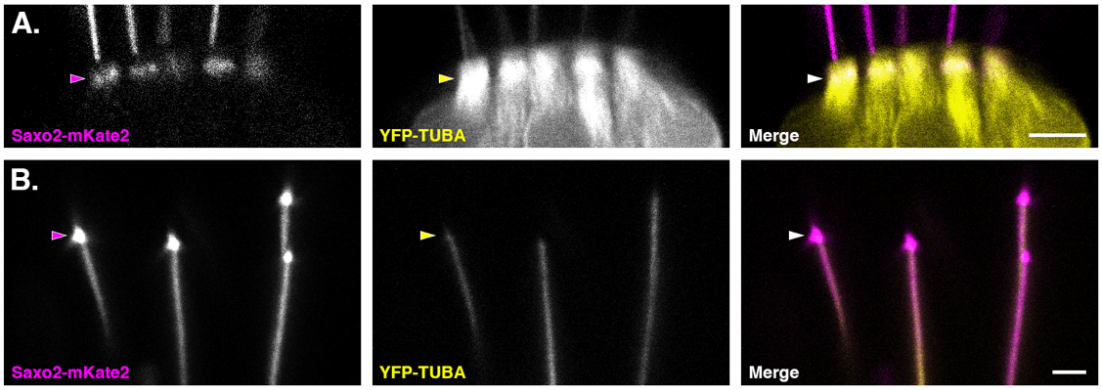

Figure S6. Details of Saxo2-mKate2 and YFP-TUBA co-localization in the subcuticular zone (**A**) and at the distal tip of kinocilia (**B**) in the lateral crista at 6 days post fertilization. Scale bar is 5 µm in A and 2 µm in B.

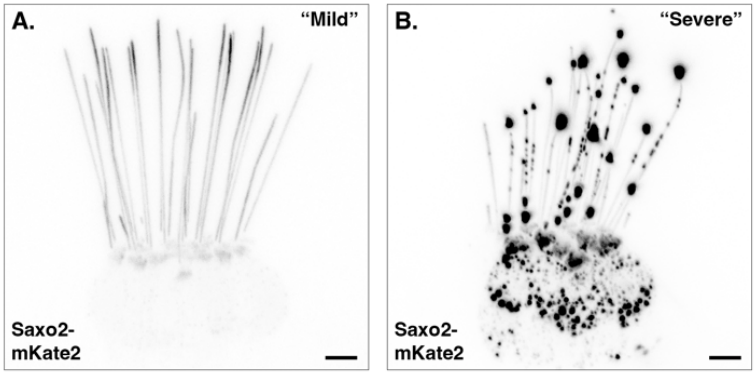

Figure S7. Comparison of fluorescent protein intensity levels in Saxo2-mKate2 "mild" (**A**) and "severe" (**B**) transgenic lines at 6 days post-fertilization. The image in panel B was captured at 88% the gain of that in panel A, thus slightly underrepresenting the true intensity difference between the two lines. Scale bars = 5 µm**.**

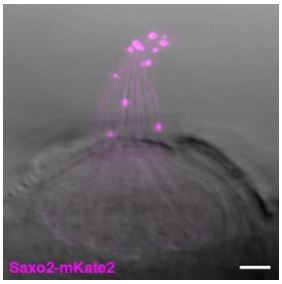

Figure S8. Example of the "severe" phenotype in a neuromast of a *saxo2-mKate2* transgenic at 5 days post-fertilization. Scale bar = 5 µm.

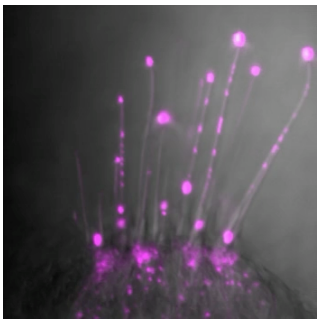

Video S1. Movement of Saxo2-mKate2 positive punctae in the kinocilia of lateral crista hair cells in a 5 dpf zebrafish larva. Note the bi-directional motion of the puncta on the left. Video info: 20 frames over 60 sec, played back at 7 fps, depth of 4.7 µm, frame dimension 40x40 µm.